Simulation Modelling Practice and Theory 142 (2025) 103107

Contents lists available at ScienceDirect

Simulation Modelling Practice and Theory

journal homepage: www.elsevier.com/locate/simpat

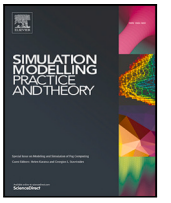

Insights into the metal cutting contact zone through automation and multivariate regression modelling under the framework of gear skiving

Florian Sauer[1,*], Amartya Mukherjee[1], Volker Schulze

Karlsruhe Institute of Technology - Institute of Production Science wbk, Kaiserstraße 12, Karlsruhe, 76131, Baden-Württemberg, Germany

ARTICLE INFO

Keywords:
Chip formation
Regression modelling
Automation
FE simulation

ABSTRACT

The modern time of Industry 4.0 requires an enhanced prediction process for reliable and sustainable manufacturing. It is essential to understand the relationships between various process parameters of machining for better optimization. Digitalization offers the opportunity to accelerate the prediction process using different modelling such as numerical and data-driven models. Improvements in the knowledge of thermo-mechanical variables and the use of finite element method (FEM) tools and machine learning approaches for thorough thermo-mechanical analysis are noteworthy contributions to the area. However, an ideal standardized approach remains to be resolved. Therefore, this research proposes a development process of an automated FEM tool to simulate the tool-chip interaction for AISI4140 material, coupled with a hybrid multivariate regression model for fast prediction of non-linear relationships between the cutting parameters and the contact properties. Consequently, the study also interprets the tool-chip interactions in the secondary deformation zone, facilitating process optimization for improved machining performance.

1. Introduction

Manufacturing sustainability is the focal point behind the abrupt change in how products are designed, developed, and delivered. In the simplest terms, sustainable production is about reinventing the entirety of the manufacturing ecosystem, dependent on its environmental footprint. Since machining is particularly essential in production processes, it incorporates a variety of aspects that have a significant influence on eco-friendly manufacturing.

Narita and Fujimoto [1] developed an analytical approach to comprehend the impact of several machining factors, such as tool wear, coolant consumption, and metal chip forms on environmental burden. Although researchers have developed multiple techniques to predict the effects of machining factors on sustainable manufacturing, an ideal prediction process still needs to be standardized [2]. Having said that, it is unanimously agreed that software technologies are vital to advancing lean manufacturing [3].

Experimental research provides valuable insight into the relationships between different process parameters and the cutting process. Yet, a more in-depth assessment of the impacts of process factors is often desired. In the era of Industry 4.0 and digitalization, computational modelling provides engineers with valuable tools to thoroughly analyse and tune machining parameters, whether in

* Corresponding author.
E-mail address: florian.sauer@kit.edu (F. Sauer).
URL: https://www.wbk.kit.edu (F. Sauer).
[1] Florian Sauer and Amartya Mukherjee contributed equally to this work.

https://doi.org/10.1016/j.simpat.2025.103107
Received 20 November 2024; Received in revised form 7 March 2025; Accepted 17 March 2025
Available online 16 April 2025

real-time or for future operations as discussed by Cimino et al. [4]. Numerous significant contributions to the field of computer simulations can be observed. Influential work by Arrazola et al. [5] enriched the understanding of the thermo-mechanical variables like stress, strain and temperature by avoiding experimental measurement difficulties. Multiple research has been conducted to analyse different aspects of high-speed machining such as separation criteria [6], impact of the tool geometry, tool coating, and cutting regime factors on the distribution of residual stress [7], examination of heat production and temperature prediction in metal cutting [8]. Other studies put forward strategies to address numerical challenges associated with computational techniques in machining simulation [9]. In modern times, the use of intricate cutter geometries during machining processes leads to the generation of three-dimensional (3D) cutting forces that pose challenges in terms of both analytical and numerical modelling. Hence, the use of two-dimensional (2D) orthogonal cutting conditions has the potential to significantly decrease model complexity and computing strain. Orthogonal cutting is distinguished by the presence of a cutting edge that is oriented at a right angle to the cutting velocity [10]. This simplification thus approximates the feed rate as the uncut chip thickness (h), the gap between the tool tip and the workpiece's edge. Additionally, for a 2-D orthogonal cut mechanics, the unit depth of cut correlates to the reaction forces that emerge in the form of N/mm [11]. Multiple studies have been conducted to research the material flow stress throughout the chip production process during orthogonal machining [12,13]. All this research highlights the necessity of FEM tools for comprehensive thermo-mechanical investigations in machining, making them essential assets in both research and industrial applications.

However, it is observed that with the automation of modern computational methods and numerical models has enabled more precise, optimized and faster analysis of machining operations. Consequently, it offers the possibility to create huge datasets for modelling data-driven approaches. The present era of big data and advanced regression analysis techniques represents the latest stage of advancements in the field of machining. Several data-driven methodologies, including curve fitting of analytical models [14,15], neural networks [16], genetic algorithms [17], random forest regression [18], and other machine learning methods, have recently been applied to transform machining processes through the use of massive datasets and complex regression models. By considering machine learning algorithms and real-time databases, the machining industry intends to reduce the cost and increase the efficiency of result generation. That said, the existing state of the art does not offer a complete architecture to combine different prediction models that provide a holistic framework for using process parameters to simultaneously predict multiple thermo-mechanical contact properties.

This evolution from analytical methods to sophisticated prediction techniques is particularly relevant for gear skiving, a complex machining process where the precise prediction of cutting forces, chip geometry, and tool-workpiece interactions is critical for optimization. For instance, previous research has conducted an in-depth study of the process kinematics of gear skiving to develop a numerical model to predict cutting forces in the gear skiving process [19] or to develop an analytical model to optimize the extreme conditions [20]. Schulze et al. [21] also used FEM to simulate cutting forces and chip formation in gear skiving, focusing on kinematic complexities. Guo et al. [22] proposed an analytical model for tool design to predict interference-free cutting conditions in gear skiving. Antoniadis [23] adapted CAD-based force prediction from gear hobbing to skiving contexts, demonstrating the versatility of force modelling. Other studies such as Bergs et al. [24] have presented an analytical kinematics and numerical simulation algorithm to calculate maximum chip thickness. However, more recent studies have used Particle Swarm Optimization (PSO) and Backpropagation (BP) neural network approach to predict and optimize geometric deviations in skiving parameters [25]. Together, these studies show how an all-encompassing predictive framework may be used to tackle the complex problems associated with gear skiving.

Thus, this study aims to propose a schematic of a FEM automation tool to accurately simulate the dynamic contact interactions occurring between the tool, chip, and workpiece in the orthogonal cut under the framework of gear skiving. In addition, the work aims to incorporate a data-driven approach in order to predict nonlinear relations between various cutting parameters and output results such as cutting forces (F_c, F_p), contact length (l_c), sticking length (l_s), contact zone temperatures (T_c), normal stresses (σ_n), and relative sliding velocity (V_s). A multivariate hybrid regression model is considered due to the multifaceted nature of prediction results, which cannot be predicted using a single sort of model. In the end, the paper focuses on studying tool-chip contact interactions in the secondary deformation zone to analyse thermo-mechanical properties, facilitating process optimization for enhanced machining outputs.

2. Materials and methods

2.1. Experimental setup

The orthogonal turning tests were carried out using a 3-axis milling machine of type POSmill CE 1000 under dry air cooling conditions as shown in Fig. 1. The workpiece is clamped in the tool spindle and the cutting speed is set via diameter-dependent rotation speed. The tests were carried out using samples of AISI4140 with dimensions of $\varnothing 120 \times 4$ mm, which were previously quenched and tempered at 600 °C for one hour in accordance with DIN EN ISO 18265. The resulting hardness is 339 ± 10 HV30, which gives a tensile strength of 1070 ± 31 MPa according to DIN EN ISO 18265. The material's chemical composition is given in Table 1. The different rake angles can be set by rotating the upper part of the toolholder, which is clamped to the Kistler Type 9255 dynamometer. The forces are recorded with a frequency of 10 kHz in direction of cutting force (F_c) and passive force (F_p) during the experiments. An algorithm was developed to filter and average only the steady-state component of F_c and F_p.

As cutting tool, a carbide insert with a Alcrona Pro coating from Oerlikon Balzers and a bulk material of type K30 according to ISO513 were used. The geometrical properties of the cutting edge are a constructive rake angle of $\gamma = 0°$, a clearance angle of $\alpha = 3°$ and a cutting edge rounding of $r_\beta = 20$ µm without chip breaker. Since the orthogonal cut is an excellent experimental

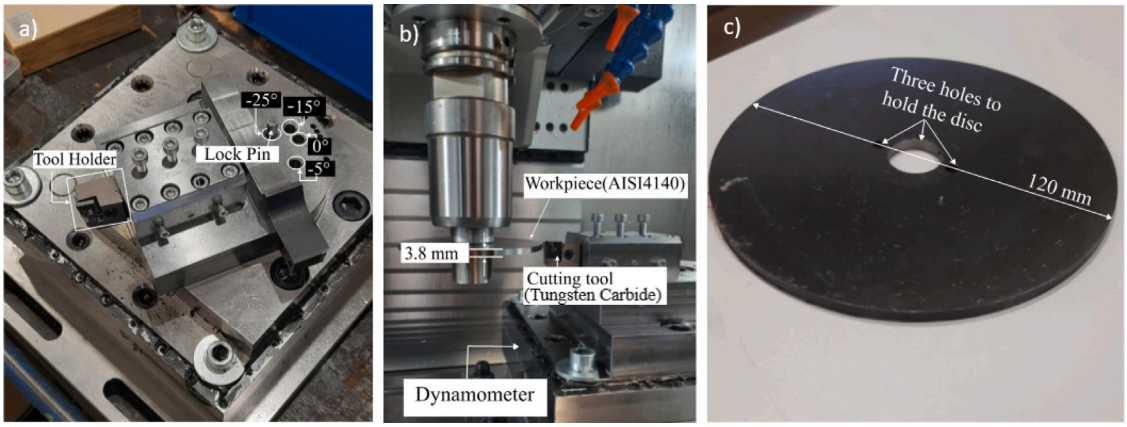

Fig. 1. Experimental setup (a) Cutting tool setup (b) Closeup of experimental configuration (c) Workpiece sample.

Table 1
Chemical composition of AISI4140 steel (wt%).

C	Mn	Si	P	S	Cr	Mo	Cu
0.41	0.81	0.33	0.01	0.023	1.04	0.189	0.13

Table 2
Workpiece, tool and process data of the investigated gear skiving process according to [27–29].

Workpiece	z_2	β_2 in °	$d_{a,2}$ in mm	$d_{f,2}$ in mm	α_n in °	$\chi_{E,2}$	b_2 in mm	m_n in mm
	−96	22.54	135.8	143.2	17.5	0.138	27.2	1.34
Tool	z_0	β_0 in °	$d_{a,0}$ in mm	$d_{f,0}$ in mm	α_n in °	γ in °	τ_0 in °	m_n in mm
	48	−0.03	68.68	60.4	17.5	0	0	1.34
Process	Σ in °	Σ_e in °	$\beta_{w,0}$ in °	$\beta_{w,2}$ in °	α_{wn} in °	$\theta_{w,0}$ in °	$d_{w,0}$ in mm	$d_{w2,}$ in mm
	−24.75	−22.48	0.026	22.45	16.81	10.63	64.08	138.68

setup for analysing complex manufacturing processes and understanding the local acting mechanisms on the cutting wedge, the characteristic process parameters of a gear skiving process were reproduced. Using the freely available OpenSkiving [26] software, parameter fields for an e-mobility internal gear (as shown in Table 2) as described by Sauer et al. [27], Arndt et al. [28], Hilligardt and Schulze [29] were calculated and analysed. Fig. 2 shows in detail the maximum, respectively minimum values along the tool contour of the considered gear skiving process for the ten tool passes.

Fig. 2(b) further shows at an example point of the tooth of the analysed gear skiving tool the local change of the cutting parameters over the tool engagement time. It can be seen, considering the orthogonal cut, that the transfer of local acting parameters over the time can therefore be a method of approach. The maximum and minimum values determined for the process parameters of the orthogonal cut — cutting speed v_c, chip thickness h and rake angle γ — were then converted to a test design with stationary parameters.

Factorial DOE is a good choice to create the initial dataset for validation purposes since the designs consist of discrete possible levels and avoid randomization. Using the central composite design (CCD) that involves the factorial points, axial points and centre points as well, which leads to a balanced representation of the design space. Therefore the following ranges were taken into account, $-25° < \gamma < -5°$, 115 m/min $< v_c <$ 140 m/min and 0.05 mm $< h <$ 0.15 mm.

As a consequence, 15 data points were generated using CCD (shown in Fig. 3), allowing the simulation to be validated to the extreme situations, where it is predicted to yield deviating findings based on literature [30–32].

To neglect the influence of wear, the cutting inserts were only used once per trial. Each test point was repeated three times to exclude influences of the test setup and for the purpose of statistical validation. Which results in a total of 45 experiments to validate the cutting forces, passive forces experienced by the tool. Furthermore, by randomizing the sequence of conducting the experiments ensured to minimize the influence of unidentified errors.

Apart from that, for measurement and validation of contact length, 15 more experiments were performed with tools having micro-textured imprints on the rake face as demonstrated by Ellersiek et al. [33]. This method has proven to be effective for instrumentation measuring the real contact length (l_c). The research indicated that this technique is especially useful for cases with high uncut chip thickness h, causing high normal stresses σ_n in the contact region, enabling accurate measurement of the contact length l_c.

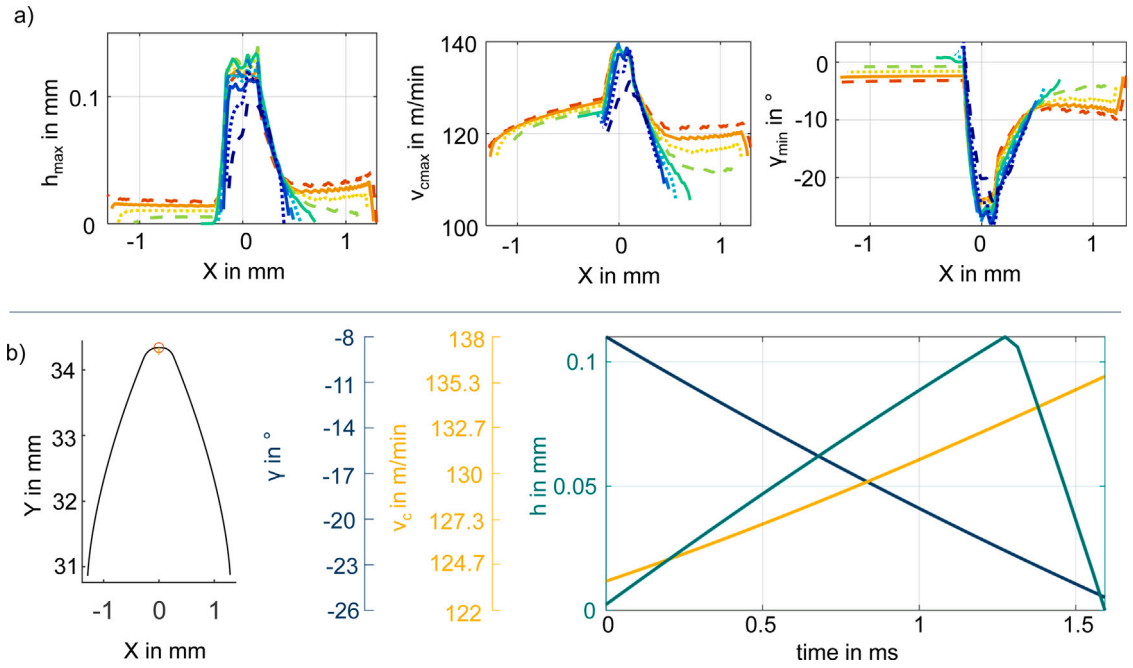

Fig. 2. Analysed gear skiving process (a) Maximum and minimum process parameters to transfer to the orthogonal cutting (b) Time dependent change of v_c, h and γ at the tool point 0 mm.

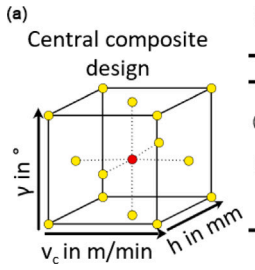

(b)

No.	1	2	3	4	5	6	7	8	9	10	11	12	13	14	15
v_c (m/min)	115	140	115	140	127.5	115	140	127.5	127.5	127.5	115	140	115	140	127.5
h (µm)	50	50	150	150	150	100	100	50	150	100	50	50	150	150	100
γ (°)	-5	-5	-5	-5	-5	-15	-15	-15	-15	-15	-25	-25	-25	-25	-25

Fig. 3. (a) Central composite design (b) Represented test points.

According to the set test programme of this study, where also low uncut chip thicknesses were tested, a slight change was made to the approach. Therefore, the position of the micro-texture were moved as close as possible to the cutting edge, as shown in Fig. 4a. The micro-textures were applied in the direction of chip flow on the rake face of the tool with a depth of 8 µm and a width of 50 µm. The gap between each textured is 100 µm. The textures are created at a steady angle, which in turn makes each strip 10 µm away from the cutting edge. Once the chip started flowing, it was observed that the micro-textured were imprinted on the back side of the chip. Consequently, once the number of strips imprinted on the chip was identified, the distance between the cutting edge and the top end of the micro-textured strip on the cutting insert represented l_c as shown in Fig. 4. The number of strip embossing was recognized and counted using a Nanofocus μsurf 3D confocal microscope. In this case, an objective with a magnitude of 20x for the chip surface and an objective with a magnitude of 50x for the cutting tool, a numerical aperture of 0.4, and a resolution in the height direction of 6 nm was used. In Fig. 4, it can be observed that inverse imprints of the micro textures of the tool in the chip surface. As the figure shows, there is no selectivity of the texturing shown. In the analyses, impressions of up to 5 µm were considered as "blur".

In addition, temperatures were measured in the tool to further and thus fully validate the simulations. Using electrical discharge machining, bores with a diameter of 0.3 mm, to fit thermocouples of Type K with a diameter of 0.25 mm, were made in the tools at geometrically defined points according to Fig. 4(b). As shown in the figure, the holes are used to measure temperatures at two positions: T_1 is the measured near to the rake face and T_2 indicates the boundary temperature for the simulation Therefore, this study performs five experiments to validate the temperature results from the numerical models and ensure the accuracy of thermal property predictions. This work considers a half factorial test design in order to verify that the simulated temperatures are within an acceptable range. Cases 1, 5, 13, 14, and 15 were chosen from the central composite design of experiments for this purpose.

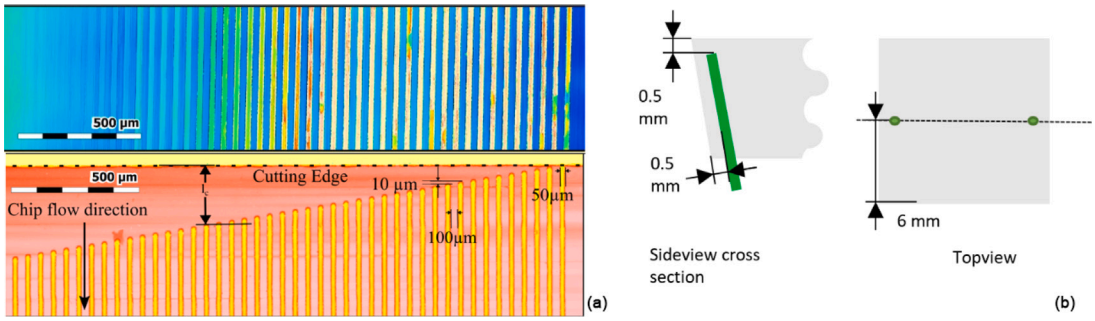

Fig. 4. (a) Analogy between the micro-textured rake face and emboss on the chip (b) Computer-aided drawing of cutting tool for temperature measurement Ellersiek et al. [33].

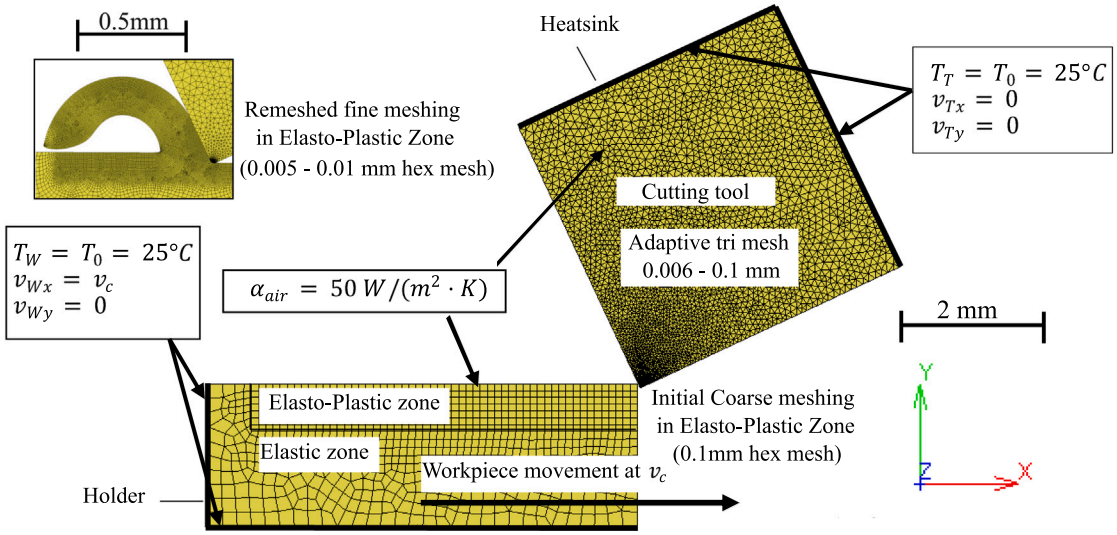

Fig. 5. Initial geometry and boundary conditions of simulation setup.

2.2. Simulation setup

The Finite element (FE) modelling was performed using a commercial software package MSCMarc [34] solver and the pre- and post-processor MENTAT. MARC uses the updated Lagrangian formulation in conjunction with continuous remeshing. A multifrontal direct sparse solution employing the entirety of the Newton–Raphson iterative procedure was utilized. In order to simulate the cutting process with a high degree of accuracy, the time step size was determined by the minimum element edge length and cutting speed.

The remeshing is dependent on strain change in the elements, which when exceeds the predetermined threshold, a new mesh is created. Since during remeshing the current state of the new mesh is interpolated from the previous mesh state, high frequency of remeshing can lead to deviations in the result as shown by Klocke et al. [35]. Hence, remeshing was conducted at every fifth increment in order to ensure the preservation of element quality, thereby ensuring the generation of valid results. Outputs were extracted at every fourth increment, thereby achieving an effective balance between the requirement for accurate data and the necessity for remeshing.

The simulation setup for the two-dimensional orthogonal cutting process, consists out of five objects as shown in Fig. 5, which are: the cutting tool, an elasto-plastic part of the workpiece, an elastic part of the workpiece, a holder, and a heat sink. The geometry used in this simulation is widely recognized and has been successfully employed in multiple studies [30,31,36], which consistently produced validated results. Leveraging this well-established geometry ensures confidence in the reliability and accuracy of the simulation outcomes, as they align with experimentally verified data. The simulation features a cutting tool fixed in space (v_{Tx},v_{Ty} = 0) with a heat sink exhibiting a surface temperature of 25 °C (T_T). The temperature and velocity boundary condition of the workpiece is given by the workpiece holder. Therefore, the resulting velocity's can be described as v_{Wy} = 0 and $v_{Wx} = v_c$, and the thermal boundary condition as T_W = 25 °C. The cutting tool is meshed with an adaptive mesh size with a minimum element edge length of 6 µm in the area of interest. This approach is consistent with studies such as, [27,30] particularly in the contact area between the chip and tool.

Table 3
Johnson–Cook Parameter.

A (MPa)	B (MPa)	C (–)	n (–)	m (–)
595	580	0.023	1.03	0.133

Table 4
Temperature dependent Thermo-Physical properties of the investigated AISI4140.

T in °C	E in MPa	ρ in kg/m^3	c_p in J/kg K	λ in W/mK	α in 1/K	ν in (–)
20	212 000	7834	–	42	1.15E−05	0.285
50	210 000	7826	464	42.4	1.18E−05	0.286
100	207 000	7811	484	42.6	1.22E−05	0.287
200	199 000	7781	522	41.8	1.27E−05	0.29
300	175 818	7748	564	39.7	1.32E−05	0.293
400	155 818	7714	616	37.1	1.37E−05	0.297
500	140 000	7678	682	34.5	1.41E−05	0.302
600	113 818	7641	780	32.2	1.45E−05	0.311
700	91 091	–	958	31.9	–	–
800	90 000	–	596	26.8	–	–

The elasto-plastic part and the elastic part of the simulation are forming the workpiece and an element type of hex-mesh with a plain strain condition. To optimize the simulation efforts, use of remeshing is allowed only in the elasto-plastic zone. The dimensions of the modelled elasto-plastic and elastic zones for the investigated material have been influenced by previous research [30,36–43], which provided the fundamental insights for this study. In case of elasto-plastic zone, the mesh size in the contact zone during remeshing process is critical for generating reliable results. A straightforward selection process of the mesh size for such a wide variety of process parameters does not always ensure optimal outcomes. Therefore, multiple mesh size conditions are considered, based on different ranges of uncut chip thickness and occasionally the cutting-edge radius. Barge et al. [9] demonstrated that optimal results are achieved by fitting 20 elements within the area of uncut chip thickness. Consequently, the minimum mesh size of the workpiece (ξ_m) is calculated using the formula $\xi_m = h/20$, where h represents the uncut chip thickness. However, for very small uncut chip thickness less than 0.02 mm having 20 elements would greatly increase computational effort hence for such cases a fixed element size of 5 µm were used. To reduce the computational effort of the simulation, only the plastic part is subjected to deformation and re-meshing. This allows the stress and strain zone of influence to reach the elastic part, but with less computing time and a more accurate simulation. The heat transfer coefficient α_{air} with the environment for both the workpiece and cutting tool is set to 50 W/(m^2 K) as suggested by Stampfer et al. [30].

Material Modelling

The workpiece material composition regarding the experimental workpiece material is modelled as temperature-dependent physical properties as discussed by Richter [44], Agmell et al. [31] and Sarmiento et al. [45]. Table 4 outlines the employed temperature-dependent thermo-physical properties of the workpiece used to model the simulations. The plasticity of the plastic zone of the workpiece is modelled using the well-known and researched flow stress model for cutting simulation by Johnson and Cook [46] and Zerilli and Armstrong [47] shown in Eq. (1).

$$\sigma_f = \left[A + B\bar{\epsilon}^n\right]\left[1 + C\ln\left(\frac{\dot{\epsilon}}{\dot{\epsilon}_0}\right)\right]\left[1 - \left(\frac{\theta - \theta_{\mathrm{RT}}}{\theta_{\mathrm{m}} - \theta_{\mathrm{RT}}}\right)^m\right] \tag{1}$$

This model is widely used to analytically express equivalent flow stress σ_f in machining where $\bar{\epsilon}$ is the equivalent strain, $\dot{\epsilon}$ is the plastic strain rate, $\dot{\epsilon}_0$ denotes the reference plastic strain rate, T represents the material temperature, T_m is the melting point of the material and T_0 is the room temperature. Further, the five parameters describing the material behaviour are coefficient A denoting the yield strength, B the hardening modulus, C the strain rate sensitivity coefficient, n the hardening coefficient and m the thermal softening coefficient. The parameters were selected according to previous work done initially by Agmell et al. [31] and were adopted by Sauer et al. [37] are given in Table 3.

Along with other boundary conditions, heat is generated by the deformation of the elasto-plastic zone. Therefore, as suggested by Svoboda et al. [48] and investigated by Özel [49] and Shi et al. [50] the heat flux for plastic deformation allows Marc to convert 90% of the plastic work into heat.

The thermo-physical properties for the cutting tool are given in Table 5 for the atmospheric temperature of 25 °C according to Reeber and Wang [51], Upadhyaya [52] and Kayser [53]. The model is configured to simulate five output parameters, which are the shape of the chip, the stress–strain curve, the temperature distribution, and the cutting forces. These parameters are analogous to those observed in the experimental results.

Contact Modelling

The tool-workpiece contact modelling plays one of the most vital roles in the accuracy of an orthogonal cutting simulation model. In the extensive literature available for modelling tool chip friction, two models that are found to be a common practice are the Shear friction law and Coulomb's friction law. In this case a recent work by Holey et al. [54] is used to determine the friction behaviour

Table 5
Thermo-physical properties of Tungsten carbide.

λ W/mK)	c_p (J/kg K)	ρ (g/cc)	E (MPa)	α_r (K^{-1})
80	180.54	15.7	$7.17E{+}5$	$5.5E{-}6$

Table 6
Dependency table of total length of cut on uncut chip thickness.

Conditions	Total length of cut l_{cut} (mm)	First length of cut l_{cut1} (mm)	Second length of cut l_{cut2} (mm)
$0.01 \leq h < 0.05$	2.5	1	1.5
$0.05 \leq h < 0.1$	3	1	2
$h < 0.1$	3.5	1	2.5

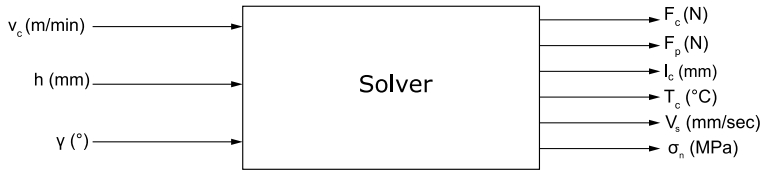

Fig. 6. Considered in- and output of the simulation.

using a multiscale approach under the framework of skiving parameters are suggesting a Coulomb friction law as shown in Eq. (2) with a varying friction coefficient μ and shear stress k depending on the normal stresses applied to the contact and therefore the frictional stress τ_f.

$$\tau_f(\sigma_n) = \begin{cases} \mu(\sigma_n)\sigma_n, & \sigma_n < \sigma_Y, \\ k(\sigma_n), & \sigma_n \geq \sigma_Y, \end{cases} \tag{2}$$

Further, the heat transfer coefficient between the formed chip and tool is given as a constant parameter as suggested by Özel [49] and set to $5E+5$ W/m^2 K.

Simulation Methodology

The fact, that only a fraction of the realistic cutting time of the orthogonal cut is being represented by the simulation, some additional conditions are taken into account to reach the thermal steady state for an appropriate representation of the experiments. The chosen strategy, consisting of a two-step simulation process, for faster attainment of the thermal steady state while maintaining the accuracy of the outcomes. A study conducted by Lorentzon and Järvstråt [55] has proposed a way of lowering the tool's specific heat capacity to achieve the tool's experimental temperatures faster within the simulations. This work adopts this idea and splits the simulation into two parts and follows the strategy shown in Table 6. By default, the total cutting length also known as the length of cut (l_{cut}) is set to 3 mm.

The simulation is implemented in two-step. The first step of the simulation has a length of cut (l_{cut1}) of 1 mm, with the cutting tool specific heat capacity (c_p) set to almost zero of 2.3 $E{-}7$ J/(kg K) to ensure numerical stability of the simulation. After the first simulation ends, the results of the first simulation are transferred to the second step with steady-state temperature condition of the cutting tool. According to Table 6 the second cutting simulation is started with the desired length of cut (l_{cut2}) and the heat capacity c_p is set to 180.54 J/(KgK) referring to Table 5. Once simulation step two is finished the post-processing of the results of interest, in detail the cutting force F_c, passive force F_p, contact length l_c, normal pressure distribution σ_n, temperature in contact T_c and the sliding velocities V_s are extracted (Fig. 6).

2.3. Automated tool setup and regression modelling

Development of successful prediction models can only be achieved through effective database production. This study focuses on developing an automated setup to generate a comprehensive database of input and output parameters (see Fig. 6). The setup fully automates the creation and result extraction of a wide range of simulation models and therefore generating the needed databases for training regression models as illustrated in Fig. 7. This allows to develop a data-driven prediction model, that minimizes the calculation time of the contact behaviour during machining, since the finite element-based numerical simulations are known to be very computationally costly and time-consuming. Depending on the input parameters, the automated workflow required 45–120 min to successfully execute the FE-simulation model. The automation part of this workflow encompasses the following:

- Iterative generation of FE models over the wide range of input process parameters.
- Automated data extraction of the key output parameters, eliminating manual post-processing and reducing human errors.

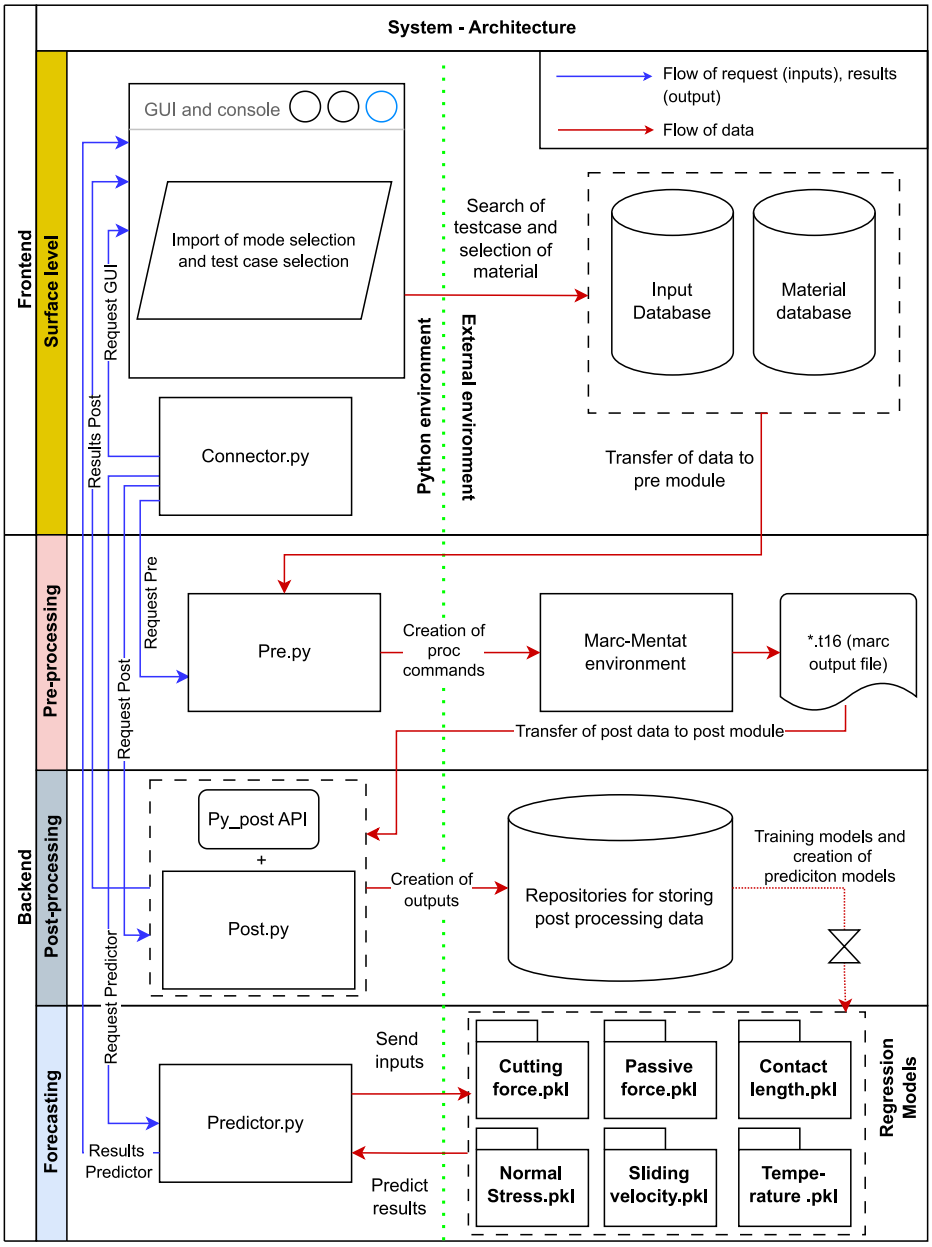

Fig. 7. Schematic diagram of the simulation setup.

- Integrated regression models accelerate the prediction of complex, non-linear relationships between input parameters and thermo-mechanical properties.

Additionally, this script-based tool offers flexibility and control to accommodate various new requirements. A basic graphical user interface (GUI) exists to toggle between pre-processing, post-processing and forecasting modes. The following section explains the software architecture, describing the tool's modularity:

- **Pre.py**: It is capable of handling core tasks, including the reading of user inputs from Excel (e.g. geometrical features and boundary conditions, process parameters, material selection and initial mesh size), the generation of *.proc files, the creation of FEM models in Mentat, the monitoring of execution status, and the batch processing of multiple test cases.
- **Post.py**: It uses the PyPost API to parse *.sts files, extract nodal data, normalize incremental data, compute mean values, and export results as plots or *.csv files.
- **Predictor.py**: Loads trained models from *.pkl files for output prediction. Training and testing is performed externally.

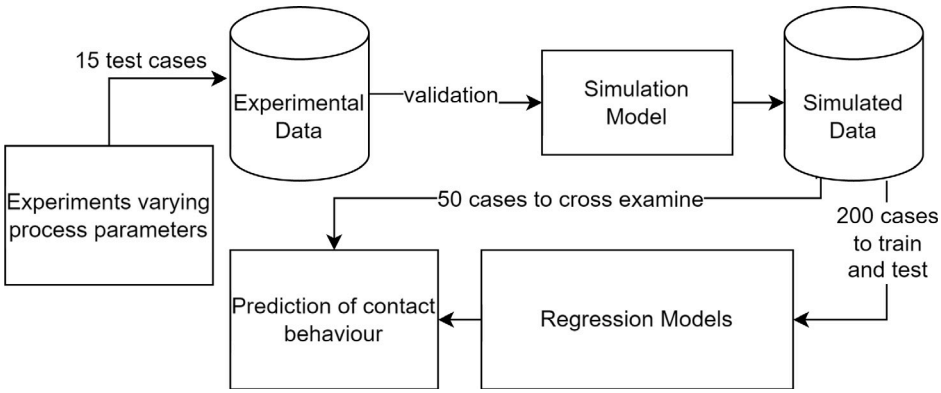

Fig. 8. Data validation workflow.

- **Connector.py**: Integrates all subprograms, providing a user interface for task selection (Pre-, Post-Processing, Forecast) and data input or test case selection.

2.3.1. Parameter identification and design of experiments

The workflow presented in the following section is a widely adopted approach in data mining processes [56]. Several studies, including those by Lostado et al. [57], Dong et al. [58] and Peng et al. [59], have employed finite element (FE) simulation models to generate initial datasets for training and testing various regression models. However, many of these studies do not offer a comprehensive approach that combines both experimental and simulation-based methods to develop more robust and valid regression models. Thus, this work encompasses all three main stages which are the experimental stage, simulation stage and prediction stage, while validating each step through a well-defined and diverse design of experiments. Therefore, multiple DOE's has been generated for each of the phases (see Figs. 8, 9).

In the earlier section, the experimental phase featuring central composite design under boundary conditions of one specific gear skiving process is already described in (Fig. 3). However, for the next phases the range of input process parameters is set, keeping the bigger picture in consideration. According to Vargas et al. [60], it is common to observe large negative local rake angles, when manufacturing external gears with small axis crossing angles. Consequently, this project primarily focuses on γ up to $-35°$, but simultaneously also considers positive rake angles up to 5° as were observed during skiving of internal gears and were investigated by Arndt et al. [28], Sauer et al. [27] and Hilligardt and Schulze [29]. To develop such a regression model capable of predicting the thermo-mechanical properties of almost all gear skiving processes, different DOEs were considered. This included training, testing, and cross-examination, with a total of 250 test cases for simulations, all within the range of the gear skiving parameter fields.

Thus, according to these conditions, the cutting velocity ranges from 100 m/min to 200 m/min and the uncut chip thickness from 0.02 mm to 0.2 mm. Among these 250 simulations, 200 were used to train and test the models and 50 were used to cross-examination the prediction quality. The cross-examination ensures that the model's performance is not a consequence of biased train–test split, but a genuine representation of its ability to make predictions to unseen data [61].

For training and testing purposes: Classical factorial experimental designs that were used in the experimental stage do not suit the deterministic nature of simulations, which produce a single output for each specific input. According to Viana [62] a strong space-filling feature is of the utmost importance because it ensures adequate coverage of the design area and enhances the likelihood of including the majority of levels for each factor. Such a sampling technique trains the models efficiently and increases the odds of accurate extrapolation of prediction models. Multiple DOEs that are independent of statistical assumptions like Hammersley, Improved Latin hypercube sampling (ILHS) are examined. However, Hammersley DOE, which has the best space-filling property, is used to create the initial 200 data points used by the automated simulation model to run on and build the database for training prediction models as shown in Fig. 9(a). According to Larson [63], the use of the same training data set for an algorithm may result in overoptimistic outcomes. Therefore, the 200 data points were partitioned using train–test tools to randomly allocate the dataset into 80% for training and 20% for testing. This ensured that the models were both trained and validated effectively.

For cross-examination purposes: The objective of the cross-examination in this study is to conduct a detailed examination of the absolute error metric, with the aim of ensuring that the prediction models are subjected to rigorous testing and validation based on their evaluation of absolute-unit deviations. As stated by Arlot and Celisse [61] the practical limitations of real-world applications result in the necessity for data splitting due to the unavailability of extensive data sets. The choice of data splitting method will inevitably result in different validation estimates. However, in this study, new data can be readily generated using the automated tool. According to Viana [62], the combination of different DOE strategies will lead to more reliable prediction models. To accomplish such a task effectively, the utilization of a stochastic design strategy is logical. This strategy ensures comprehensive testing of the models with a smaller number of runs, thus contributing to the efficiency of the process. So, Monte Carlo fits these criteria the best and is used to create the rest 50 data points that are further simulated using the automated simulation tool as shown in Fig. 9(b).

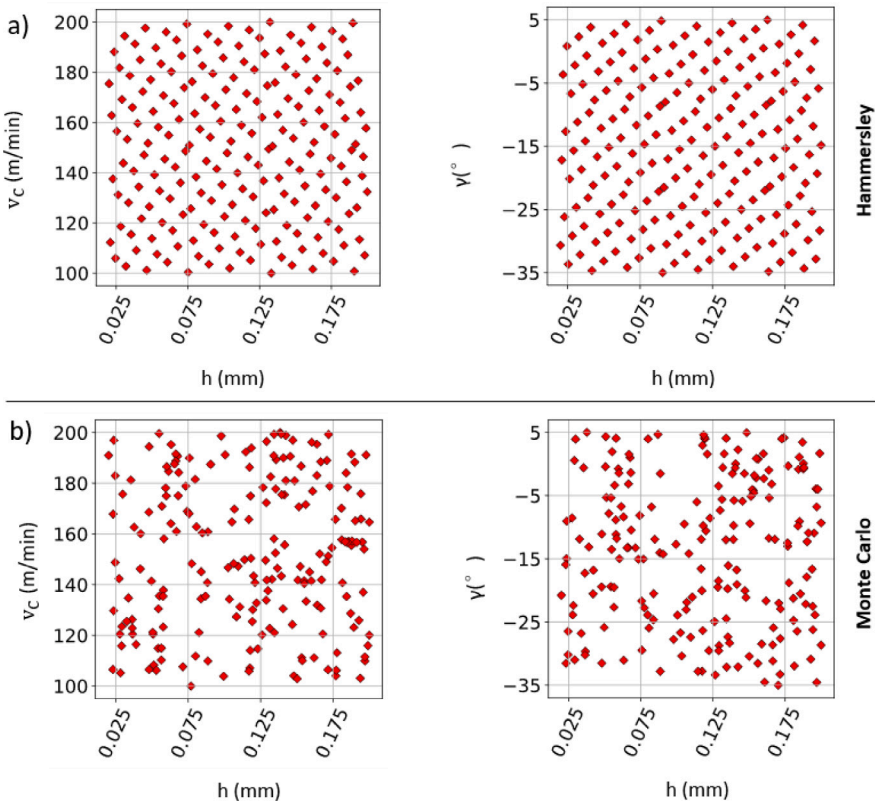

Fig. 9. Overview DOE's for simulation (a) Hammersley DOE for simulation purpose (b) Monte Carlo for Validation purpose.

2.3.2. *Architecture and implementation of regression models*

To design the architecture of the prediction models, a hybrid approach is adopted. The orthogonal cutting mechanics is a complex nonlinear system. Not all the results can be directly predicted using a conventional regression method. Hence, this work presents a novel approach which combines multiple machine-learning approaches depending on the non-linearity of the outputs and builds a system to train six models based on the range of input process parameters indicated in Fig. 10. In the realm of machine learning, the outputs are also termed dependent variables and the inputs are termed predictor or independent variables. The architecture of the model training technique is stated as follows:

Inputs/Predictors: It is discussed earlier that, the three predictors (cutting speed v_c, uncut chip thickness h and rake angle γ) are varied using Hammersely experimental (200 test cases) according to Fig. 9.

Stage 1 of Dependent variable: The model predicts the single-valued outputs in the first stage. These include the cutting normal forces, the tangential passive force experienced by the tool and the average contact length value.

Stage 2 of Dependent variable: In the second stage, the prediction criteria are not as straightforward as the prior and these are dependent on an additional pseudo predictor. As shown in Fig. 11, the thermo-mechanical properties of the contact region (sliding velocity v_s, temperature T and normal stress σ_n) are not a single averaged value but instead a non-linear curve over the contact length. Within Fig. 11, it is also illustrated that this study adopts the theoretical premise of regarding the material separation zone as the initial point for calculating the positive contact length of the chip and tool over the rake face. Consequently, the contact zone of the chip and tool on the flank side is designated as the negative contact length [37,64]. In addition to the total contact length, the sticking zone can also be identified in accordance with the description provided by Zorev [65]. The value of l_s can be calculated when the relative sliding velocity v_s of the chip is almost zero. This is the initial adhesion zone of contact, where the shear strength S_1 is $S_1 < \mu\sigma_{smin}$ [66]. Model 6 illustrated in Fig. 10 was used to predict the rate of change of sliding velocity v_s, across the contact length l_c. Later in the study, the resulting sliding velocity values were then employed to determine the stick length l_s. For such complex forecasting, the stage 2 models (model 4, 5, 6 as shown in Fig. 10) need to be trained in a discretized approach. This involves predicting the thermo-mechanical values for each discretized positional value of a specific test case scenario and subsequently combining them to form the desired curve. During the training of the stage 2 models as illustrated in Fig. 10, the models are not conditioned on a single output per each test case. Instead, training is performed using a combination of the initial predictors along with a distribution of positional values across the contact length. This positional distribution spans from 0 to the maximum contact

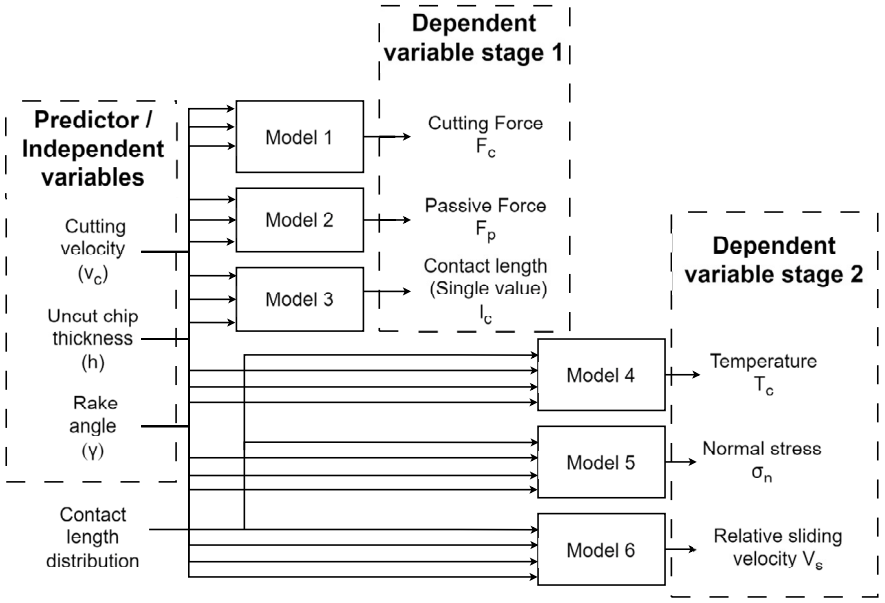

Fig. 10. Architecture of regression algorithm.

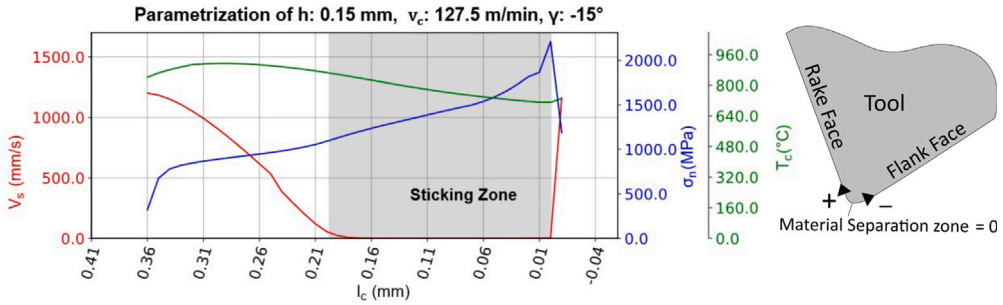

Fig. 11. Graphical illustration of contact interaction.

length value, with 10 μm intervals. Three selected methods are employed and compared for the final ecosystem: (1) curve fitting through analytical prediction models, (2) polynomial regression fitting and (3) the Random forest regression algorithm.

While curve fitting and polynomial linear regression offer better transparency and user accessibility, it is also not a suitable choice when the non-linearity between the predictor and outcomes increases. In such scenarios, the selection algorithm prioritizes Random Forest regression. Instead of constructing an equation for forecasting purposes like curve fitting and polynomial regression, Random Forest regression tackles such issues using regression trees [67]. This order of selection essentially focuses on the need for a more powerful model to capture the complex non-linear relationships, while acknowledging that the transparency declines as the algorithm progresses from curve fitting to the more obscured nature of the Random Forest regression method. Curve-fitting and polynomial models are computationally less intensive to train and maintain in comparison to the Random Forest method. Furthermore, since Random Forest, by default, assumes non-linearity of the relationship [68], it is susceptible to overfitting in the event of a linear relationship. Consequently, it is only selected when a significant non-linearity is identified between predictors and dependent variables.

The R-squared score is used as the effectiveness metric. It demonstrates how well the model is performing in predicting the proportion of variance in a dependent variable. If the collective R-squared score of the 200 test cases for the first method is greater than the criteria of 0.90 then the method is selected; otherwise, the algorithm moves to the next substantially stronger regression model as illustrated in Fig. 12. The selection algorithm is repeated six times for each dependent variable. The stage 1 models involve single-value predictions and are comparably simpler. The model developed by Kienzle [69] was utilized to predict the specific cutting and passive forces. According to the Kienzle model, a power function portrays the impact of h and v_c, while an exponential function depicts the influence of γ on the forces. The following equation was used with a curve-fitting prediction model to forecast the F_c

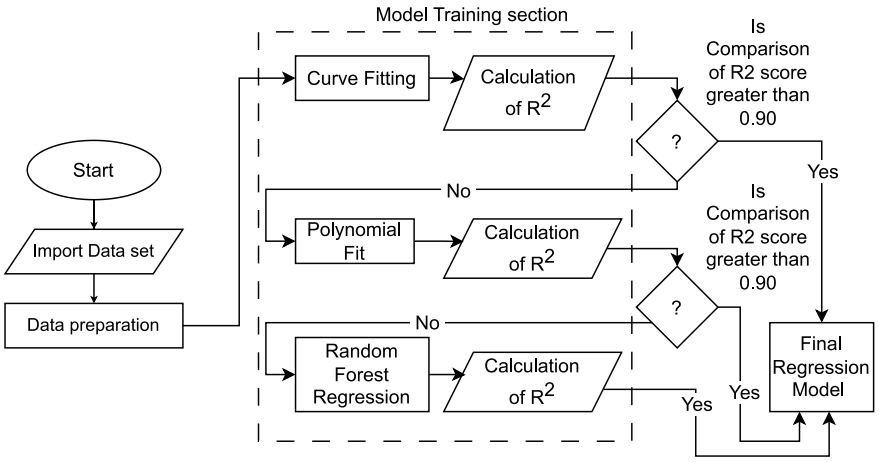

Fig. 12. Flow diagram for prediction model evaluation.

(Eq. (3)) and F_p (Eq. (4)) respectively, where, a, c_1, c_2, c_3 are coefficient of determination for the curve fitting model.

$$F_c = a \cdot v_c^{c_1} \cdot h^{c_2} \cdot e^{c_3 \gamma} \tag{3}$$

$$F_p = a \cdot v_c^{c_1} \cdot h^{c_2} \cdot e^{c_3 \gamma} \tag{4}$$

Nevertheless, identifying a suitable equation for implementing a curve-fitting model to predict contact length proves to be challenging. While this work focuses on forecasting l_c based on h, v_c and γ, it is acknowledged by Zadshakoyan and Pourmostaghimi [17] that several other factors also influence tool-chip contact. Therefore, a polynomial linear regression model with a coefficient degree of 5 was adopted to predict l_c.

As previously stated in Fig. 10, the stage 2 of forecasting deals with complex outputs that are contact zone dependent. In this stage, besides analysing single-value deviation, gradient analysis of the graphs is also necessary. A variation in the contact length leads to a change in gradient. Especially when the total contact length (l_c) is small, it causes high gradients of the T_c, σ_n and v_s results and conversely, when l_c increases, the gradient decreases. Such complex non-linearity between the predictors and outputs necessitated the use of polynomial a decision tree-based regression models. In the case of T_c, the graph exhibits a sinusoidal nature, but there is no noticeable pattern observed for v_s and σ_n. Thus, Random Forest regression was employed for v_s and σ_n, while the less powerful but more transparent model of polynomial linear regression with a coefficient degree of 6 was chosen for predicting T_c.

2.4. Utilization of the tool for gear skiving process

The developed prediction models of the 2D-abstraction of the variables of the gear skiving can be applied to predict the forces acting on the cutting edge during the actual process. The experimental results were obtained from Ref. Sauer et al. [27], using a test machine Pittler PV315 SkivLine with test specimens the same type as used in the orthogonal cutting tests as well as the same cutting rounding and tool coating. The cutting strategy consists of a 10-infeed strategy with a constant radial infeed of 10% each. The forces were recorded with a Kitler dynamometer of type 9124B during the tests. The time-varying parameters of the process under investigation as shown in Table 2, researched excessively in previous researches by Arndt et al. [28], Sauer et al. [27], Hilligardt and Schulze [29] were analysed for that purpose.

The input variables required for the prediction model, v_c h and γ, according to Fig. 10 were extracted according to Fig. 13. For each time step (tool rotation angle in the diagram), the contact length c_l and normal stress distribution σ_n, T_c and v_s were determined. In the following step, the local tangent was determined at the corresponding points of the tool and the contact length was applied orthogonal to it (cf. Fig. 2). With the specified discretization of the models of 0.01 mm, the local x and y values of the normal stress were determined as a function of the contact length and rotation angle using Eq. (5).

$$\begin{pmatrix} x_{cl_t} \\ y_{cl_t} \end{pmatrix} = \begin{pmatrix} x_{cuttingtool} \\ y_{cuttingtool} \end{pmatrix} + c_{l_{t,x,y}} \times \begin{pmatrix} x_{norm} \\ y_{norm} \end{pmatrix} \tag{5}$$

The contact area A_{cl} results from the value of the contact length and the discretization of the cutting edge therefore $\mathrm{d}A = \mathrm{d}x\mathrm{d}y$. The resulting normal force acting on the rake face of the gear skiving tool can be predicted using the information collected from the local dependent σ_n and c_l according to Eq. (6).

$$F(t) = \int \int_A \sigma_n(x, y, t)\, \mathrm{d}A_{cl} \tag{6}$$

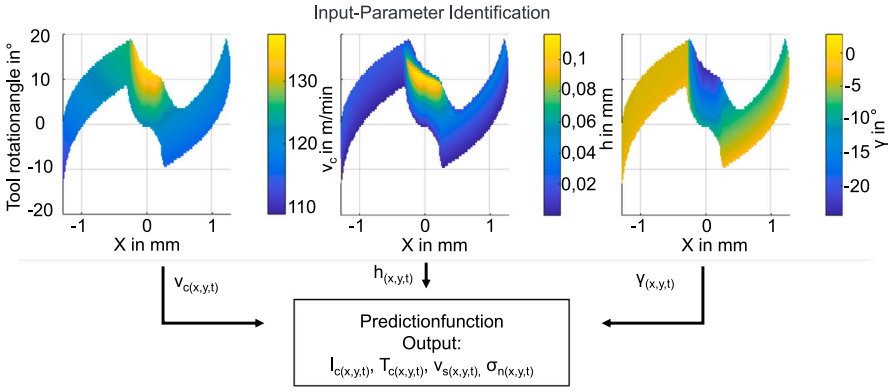

Fig. 13. Identified parameter fields of the considered gear skiving process using OpenSkiving [26].

3. Results and discussion

3.1. Evaluation of FE-simulation

The validation of the simulation is based on the following properties: F_c, F_p, l_c, T_c and h_c. Fig. 14 compares the simulated and experimental results for the 15 test cases stated in Fig. 3, providing insights into the percentage deviations.

Cutting and Passive Force (F_c, F_p) — The achieved results validate the fundamental nature of F_c and F_p : the forces increase as the h increases and the rake angle γ becomes more negative. Further, a slight decrease of F_c and F_p is noticed when the v_c increases while keeping the other two parameters constant. These observations are consistent with the results of the research of Sivaraman et al. [70] and Mustafa Özdemir and Yilmaz [71]. This general behaviour of the measured forces is also reflected in the simulations, although there is an overestimation of F_c and F_p during high negative rake angle (γ) and an underestimation for steeper rake angle (γ) conditions.

The numerical model yields more accurate simulated results for F_c, with an average deviation of 5%, compared to F_p, which has an average deviation of 12%. This is anticipated as the material flow models like those from Agmell et al. [31] and other recent studies such as Stampfer et al. [30] and Bergs et al. [32] show a similar trend.

Contact Length (l_c) — The presented experimental investigation illustrates excellent agreement with the simulation model with an average deviation of 5% with experiments and hence confirms the friction modelling for AISI4140 under the considered process parameters.

Temperature (T_c) — A comparison of experimental data and simulations indicates a satisfactory correlation, thereby validating the authenticity of the simulation model. However, it is also observed that the simulation model has overestimated the temperature values throughout the five chosen test cases. This behaviour might be due to the fact, that the temperature of T_1 in the simulation is not considering the heat transfer coefficient between the tool and the thermocouple. Further, since the T_c is placed close to the cutting zone, where also high temperature gradients are evident, even a small manufacturing error can influence the measurements significantly.

An overall comparison of the results shows very good agreement between the experimental results and the simulation results, which therefore makes the simulation suitable for regression modelling.

Chip Thickness (h_c) — Aside from the aforementioned properties, deformed chip thickness (h_c) is also taken into consideration for validation purposes. The simulations were modelled using dry friction parameters and the produced results corroborate well with the experimental values. The model overestimated h_c for all test cases with an average deviation of 12% and a maximum deviation of 20%. Given that the measurements are on the micron scale and the maximum deviations amounts to 30 µm approximately, the values are well within the acceptable limits.

Moreover, the strong correlation between the simulated and experimental results, further supports the accuracy of the chip formation model. The simulation model consistently replicates the chip thickness h_c and contact temperature T_c within the boundaries of the observed deviations.

3.2. Evaluation of prediction models

In the initial step of evaluation, the data generated with the 200 simulations are compared with the regression data obtained from the six different models, as illustrated in Fig. 15. As previously stated in Section 2.3.1, a 20% of the 200 data points was set

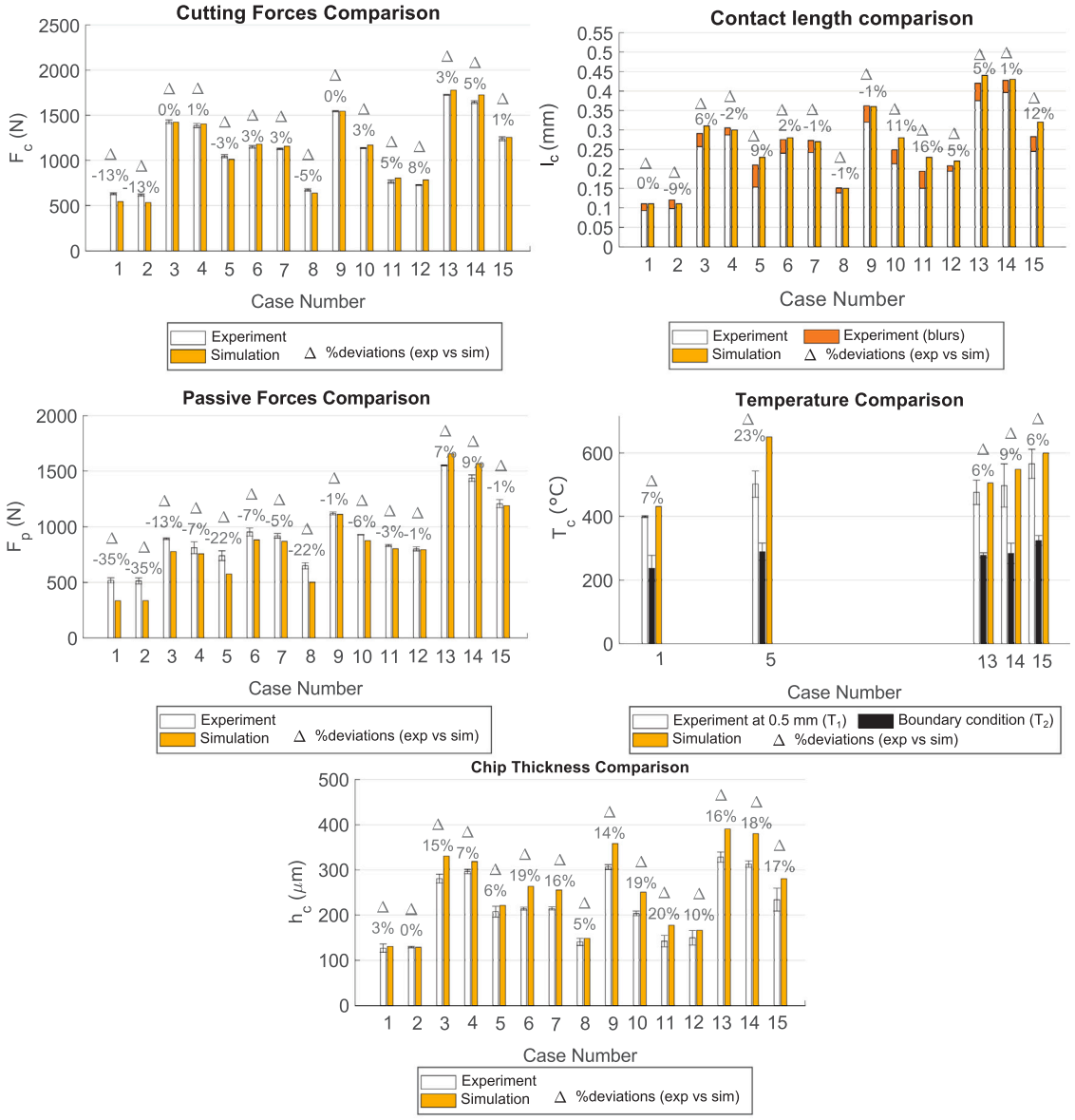

No.	1	2	3	4	5	6	7	8	9	10	11	12	13	14	15
v_c (m/min)	115	140	115	140	127.5	115	140	127.5	127.5	127.5	115	140	115	140	127.5
h (μm)	50	50	150	150	150	100	100	50	150	100	50	50	150	150	100
γ (°)	-5	-5	-5	-5	-5	-15	-15	-15	-15	-15	-25	-25	-25	-25	-25

Fig. 14. Comparison of experimental and simulation results for F_c, F_p, l_c, T_c and h_c.

aside for testing purposes, thereby ensuring that model validation was conducted on new data. The closer the data points are to the reference line, the more accurate the prediction models are. For the majority of the models, data points are close to the reference line, demonstrating the high robustness of the selected models. However, certain sections of the models deviate from the reference

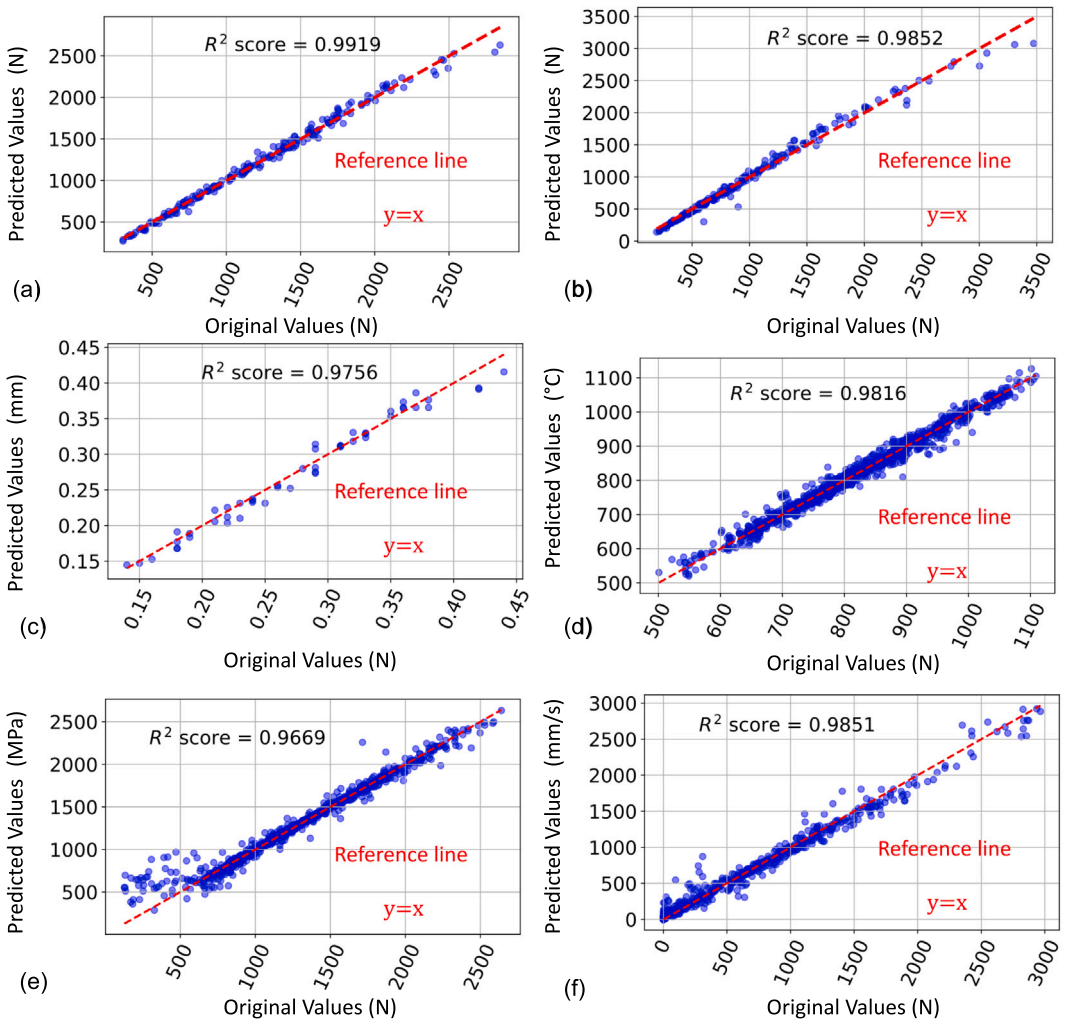

Fig. 15. Original versus predicted data of (a) F_c cutting force, (b) F_p passive force, (c) l_c contact length, (d) T_c contact temperature, (e) σ_n contact pressure, (f) V_s sliding velocity.

line. The analysis of Fig. 15 suggests that the following regression values of the respective models may deviate when (a) $F_c > 2000$ N, (b) $F_p > 3000$ N, (c) $l_c > 0.4$ mm, (d) $T_c < 650$ °C, (e) $\sigma_n < 600$ MPa or $1700 < \sigma_n < 1900$, (f) $V_s > 2500$ mm/s or $V_s < 500$ mm/s.

In the second stage of evaluation, the 50 test cases generated using the Monte Carlo experimental design were utilized to cross-examine the forecasting deviation in absolute values rather than percentages, as discussed earlier in Section 2.3.1 on the importance of absolute error analysis. Fig. 16 demonstrates the five highest deviated values for F_c, F_p and l_c. Upon further investigation of Fig. 16, it can be concluded that a combination of high h, v_c and a negative γ may result in a greater degree of deviation.

Despite the combined R-squared scores depicted in Fig. 15 being excellent, it was observed that certain test cases exhibited very low R-squared scores for the stage 2 models of Fig. 10. A thorough investigation of the 50 test cases was conducted for each output in stage 2, with selected results presented in Fig. 17. It was noted that for test cases with low R-squared scores, the actual values were not significantly deviated. For instance, Fig. 17(1) demonstrates the worst prediction scenario for temperature with a R^2 score of 0.30, but it is acceptable given its real deviation is only 50 °C and resulting in a deviation of less than 10% from the numerically simulated value.

3.3. Interaction of process parameters on contact properties

The aforementioned work has established the groundwork for the analysis of tool-chip contact interactions in the secondary deformation zone, with a particular focus on the investigation of thermo-mechanical loads. In the following section, the collinear relationship between the process parameters (inputs) and the contact properties (outputs) is investigated. In Fig. 18 shows the correlation matrix of the investigated in- and outputs. The correlation matrix indicates whether the relationship is strong linear

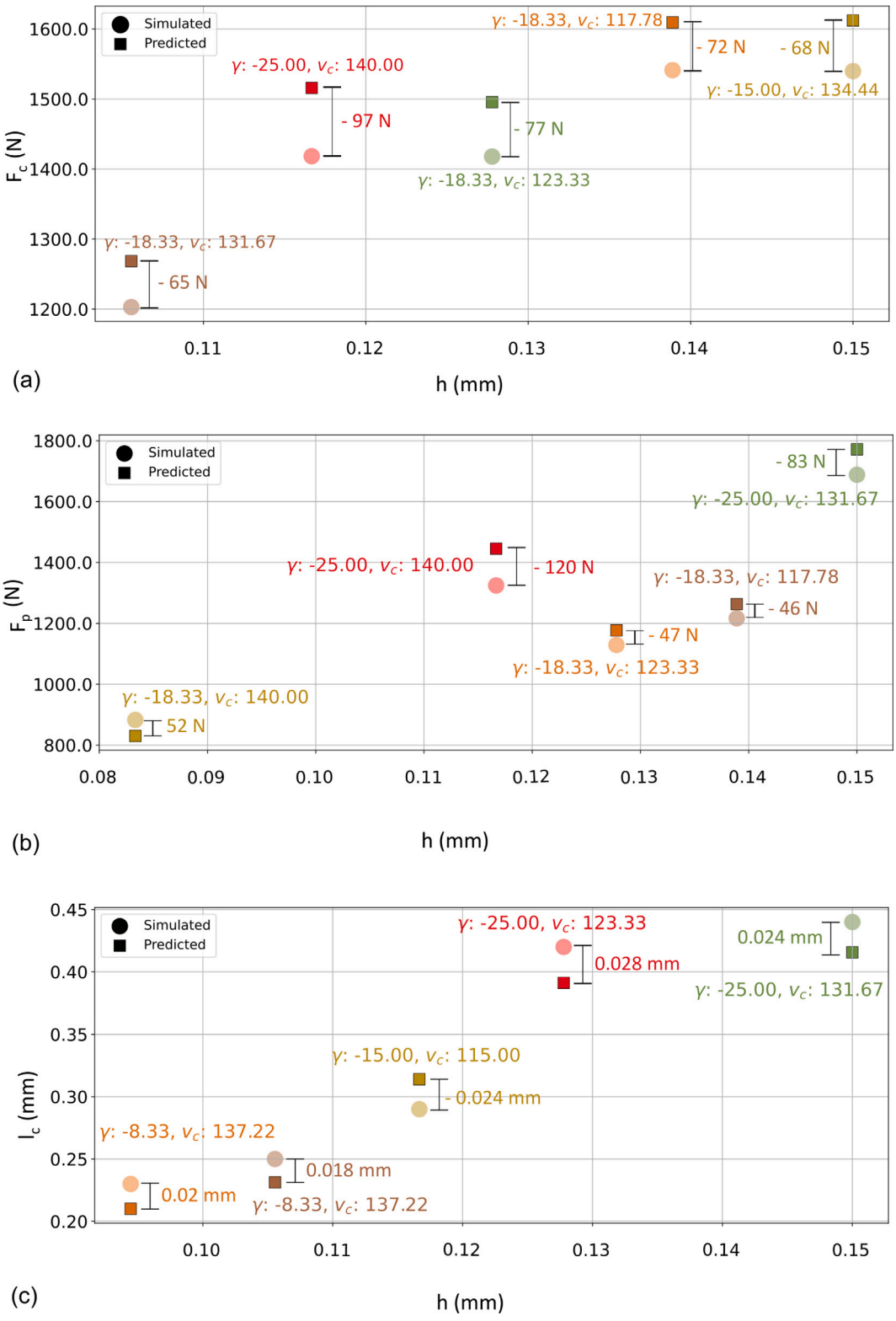

Fig. 16. Top 5 deviated test cases under cross-examination of Stage 1 models to forecast (a) F_c cutting force, (b) F_p passive force, (c) l_c contact length.

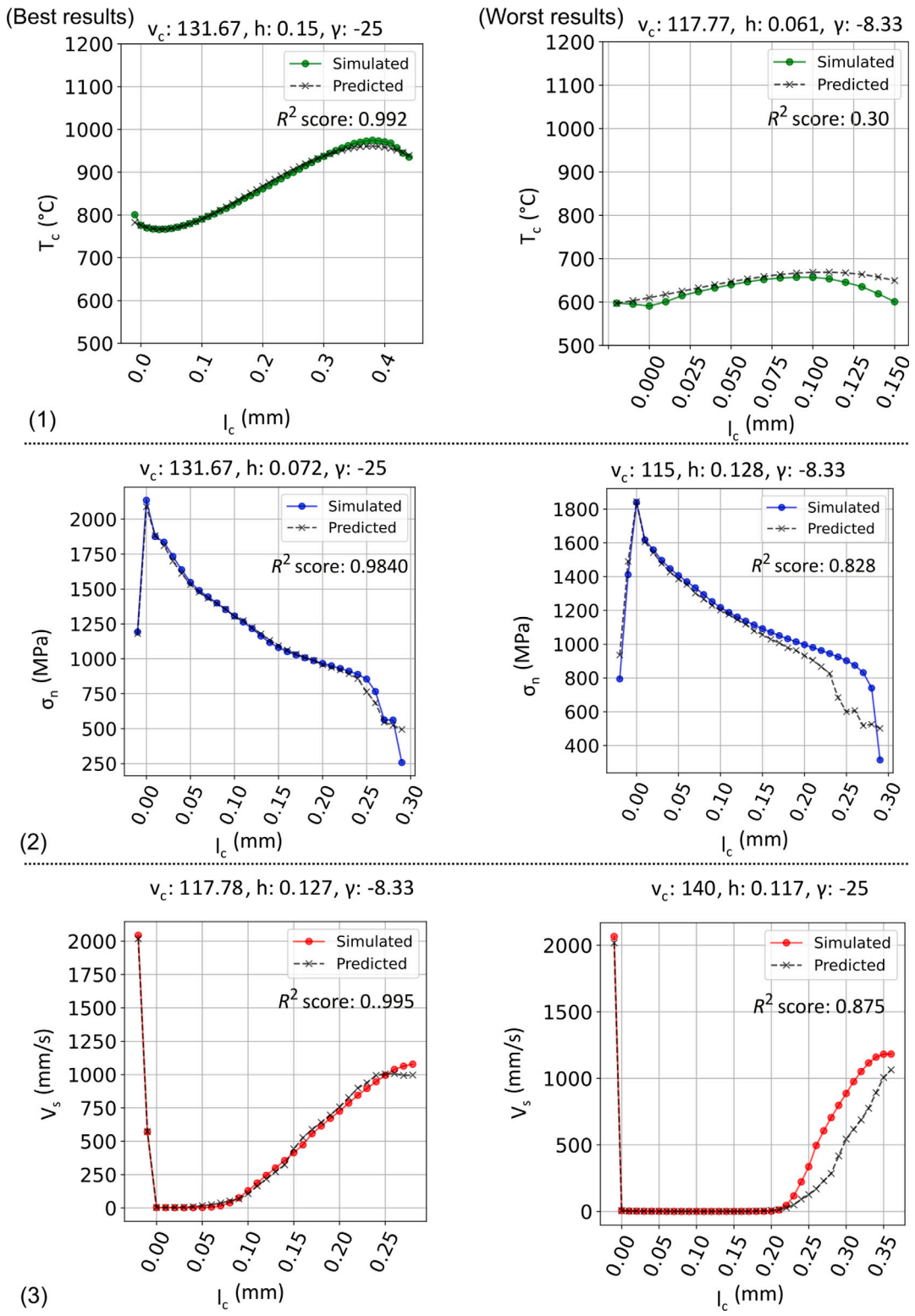

Fig. 17. Investigation of best and worst test cases under cross-examination of Stage 2 models to forecast (1) T_c contact temperature, (2) σ_n contact pressure, (3) V_s sliding velocity.

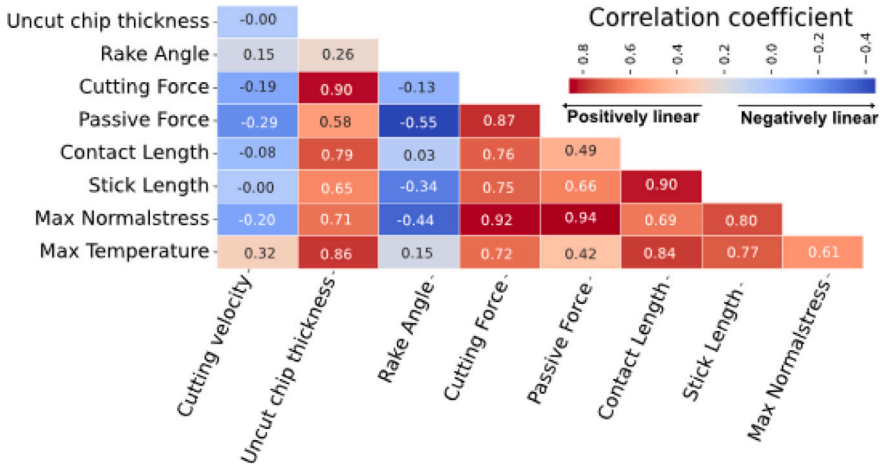

Fig. 18. Correlation matrix between input parameters and output properties.

(values close to 1 or −1) or it has weak or no linear relationship (values around 0). In addition, a positive value represents a positive correlation, whereas a negative value represents a negative one. The key insights that are observed in Fig. 18 are as follows:

Cutting Velocity v_c:

- The cutting velocity shows a minimum linear relationship, indicating that within the three considered input parameters, v_c has the least effect on the contact properties.
- For contact length (l_c) and for the sticking zone of the contact length (l_s) where the relative sliding velocity (v_s) is approximately zero or very low, v_c has almost no effect.
- A moderate negative correlation with F_p and a weaker negative correlation is present with F_c suggest that increasing v_c slightly reduces F_c and F_p.
- A notable positive correlation is observed with maximum contact temperature ($T_{c\max}$), due to higher sliding velocities and therefore higher thermal generation. According to Altintas [72], the friction power $P_u \propto v_c$. As the v_c increases, P_u also rises. Consequently, the power utilized in the tool-chip contact is dissipated in the form of heat, leading to an increase in temperature T_c.

Uncut chip thickness h:

- h plays the most significant role in determining the contact properties.
- The relationship with F_c, l_c, l_s, $\sigma_{n\max}$, $T_{c\max}$ is strong and positively linear. This indicates that thermo-mechanical properties are highly dependent on the amount of material removed and increase with the uncut chip thickness. Since higher uncut chip thickness leads to a higher required force for separation, it results in high normal stress.
- Elevated normal stress distribution within the contact area due to increased h results in greater heat generation from friction.
- Only h has a direct effect on the contact length while v_c and γ has little to no effect.

Rake Angle γ:

- The correlation between the rake angle γ and the maximum normal stress $\sigma_{n\max}$ is negative, indicating that as the rake angle tends to negative values, the contact normal stress on the cutting tool increases.
- A moderate negative correlation is observed between γ and F_p.
- No notable relationship was found between the γ and l_c, but a negative correlation was observed between γ and l_s. According to the postulates stated by Rubenstein [66], the chip adheres to the tool when the shear strength S_1 is $\sigma_{n\max} > S_1 > \sigma_{n\min}$. It continues to adhere until S_1 matches $\mu\sigma_n$. Since a higher negative rake angle increases $\sigma_{n\max}$, the chip's sticking length increases until S_1 reaches the maximum normal pressure value, as a result l_s increases.

3.4. Effects of varied process parameter combination on contact behaviour

The preliminary analysis using the correlation matrix in Fig. 18 provides a general understanding of which process parameters influence the thermo-mechanical loadings the most. Yet it does not establish the nature of correlation nor does it convey a more thorough analysis of the combined impact of multiple input parameters on the output properties. To achieve this task, this study used

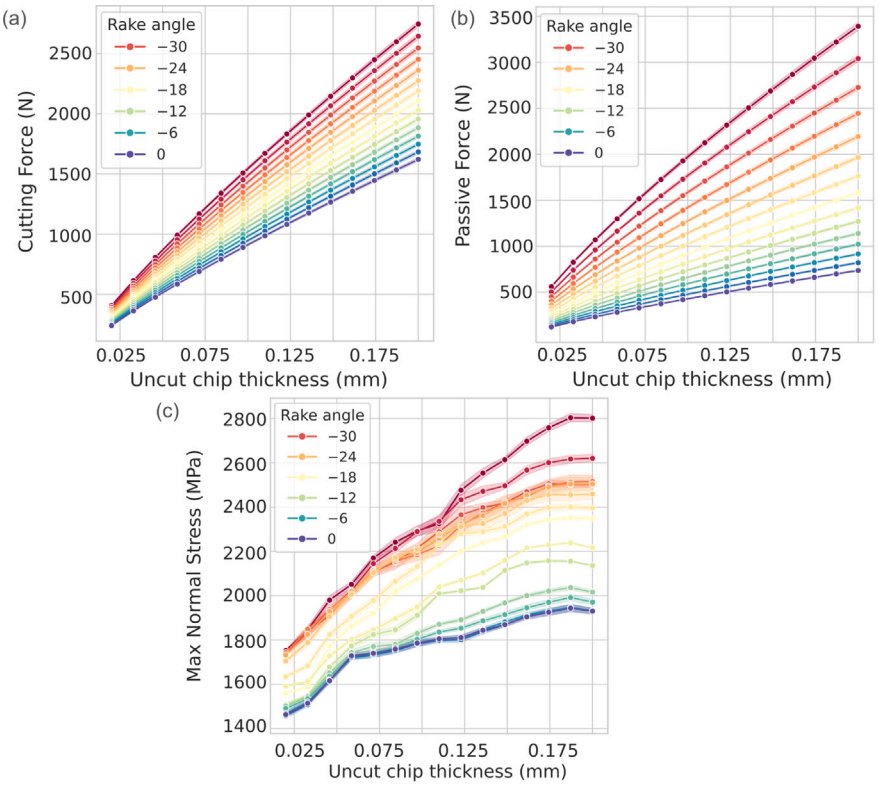

Fig. 19. Interaction plots of (a) F_c cutting force, (b) F_p passive force, (c) $\sigma_{n\max}$ maximum normal contact pressure.

the aforementioned multi-variate regression modelling to interpolate and extrapolate all points inside the considered data space. This approach served two purposes: first, to extract deeper insights and second, to verify the tool's prediction capabilities. A data space was created using an equal interval of 15 steps for each of the three input parameters, resulting in a total of 3375 test cases. For classification, one simulation is contingent upon the input conditions and ranges from 45 to 120 min. The mean simulation time is 85 min (approximately 1.42 h), which would normally entail a data production time of 276,750 min for 3375 test cases. However, the implementation of the prediction model has reduced this time to 112.5 min, thereby significantly reducing the time demand. The use of the prediction model has resulted in a time reduction by a factor of 2460 compared to the use of the FEM simulation for 3375 test cases.

3.4.1. Correlation study of investigated properties using interaction plots

Merely demonstrating a correlation is insufficient, rather the nature of the relationship is also vital. To achieve it, interaction plots were created to understand the mixed impact of the critical input parameters. In Fig. 18, it is observed that h is the most influential cutting parameter, followed by γ as the second most important process parameter to consider. Notably, for maximum contact temperature T_c, the cutting velocity v_c plays a greater influential role than γ. Hence, for the interaction plots it was decided to examine the relationship between h and the output properties, with varying metric for various γ in machining process as shown in Figs. 19 and 20. Except in Fig. 20(c) the plot shows a relationship between h and T_{cmax} with varying v_c to explore their combined effect.

Both Figs. 19 and 20(right) include a shaded band in the background of each curve. This band represents the aggregated data for repeated predictions under the same h and γ conditions but with different v_c values. The band shows the mean and the 95% confidence interval, providing a visual indication of the variability and reliability of the results. Since F_c and F_p were modelled using Kienzle model (Eqs. (3) and (4)), a linear relationship with h is expected, as long as the minimum uncut chip thickness is reached. For F_c, the data shows a consistent inclining trend showing nearly linear relationship. However, for F_p at higher h, the lines show minor deviations of linearity (see Fig. 19(b)). For each rake angle γ, the increase in F_c and F_p is fairly linear, but the slope of the lines increases as the γ becomes more negative. This shows the forces increases in a faster rate for negative γ. These initial observations of cutting forces align well with findings from previous studies by Karpuschewski et al. [73] and Salehi et al. [74].

In Fig. 19(c) the relationship between maximum normal stress σ_{nmax} and uncut chip thickness h shows more non-linearity compared to the other presented plots. While the normal stress also exhibits a similar trend of increasing with h, the lines display a notable degree of nonlinearity, particularly at higher values of h. This suggests that the increase in normal stress with uncut chip

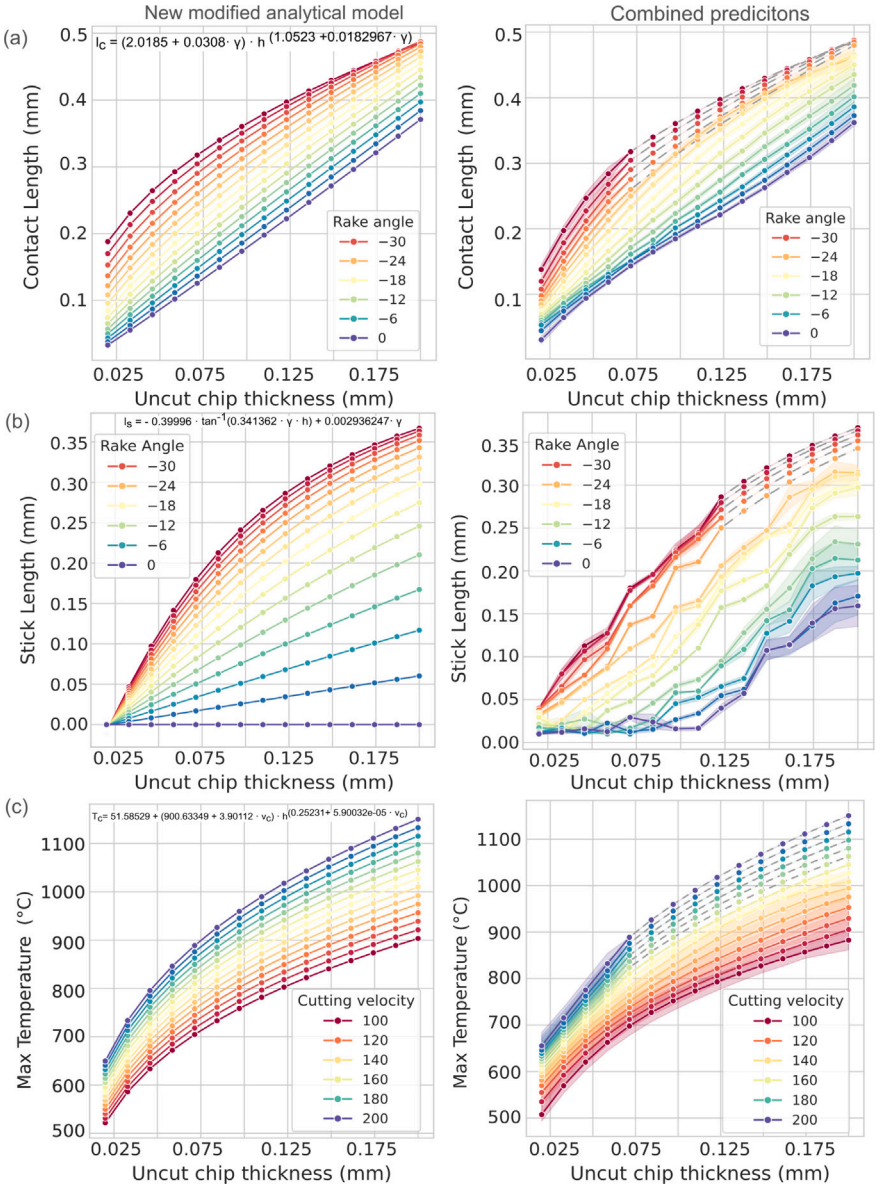

Fig. 20. New Analytical Models (left) and Interaction plots (right) of (a) l_c contact length, (b) l_s stick length, (c) T_{cmax} maximum contact temperature.

thickness h is not uniform and may plateau or even slightly decrease after a certain point. The impact of γ on σ_{nmax} is similar in trend and increases with increasing high negative γ. However, the non-linear nature of the stress increase with h makes this relationship more complex. Nevertheless, while investigating how the remaining input parameters interact with the contact properties, it was observed that three of six contact properties - T_c, l_c, l_s - failed to extrapolate accurate values under extreme conditions of γ and h. Since each of the six models were trained independently, the limitations of these three models did not cause any hindrances to the other three properties (F_c, F_p, $\sigma_{n\max}$). Yet, all the six models efficiently interpolated the values within the threshold of $\gamma < 25°$. To address the failures in extrapolation, analytical prediction models were developed specifically for the regions where the original models underperformed. The analytical models are mentioned in Fig. 20 respectively.

While, in Fig. 20(a) the contact length (l_c) increases with h, showing a predominantly linear trend, there is a slight curve at the lower h, particularly for the lines corresponding to more negative rake angles (γ). As the γ becomes more negative, the l_c increases for a given h. The data points are more spaced out at lower γ values, until h becomes considerable high level, where the influence of high negative γ becomes insignificant to increase the contact length l_c. The interaction plot of stick length l_s (see Fig. 20(b)(right)) shows a less linear trend than l_c. An initial rapid increase in l_s with h is observed, followed by a more gradual rise, particularly at higher negative rake angles γ. While at steeper γ, the initial rate of increase is slow, and after h crosses 0.125 mm barrier the rate of

Table 7
Machining parameters and their effects.

Situation	h (%)	γ (%)	v_c (%)	F_c	F_p	l_c	l_s	σ_{nmax}	T_{cmax}
1	0.5	0.2	0.3	High	High	High	High	High	High
2	0.3	0.5	0.2	Mid-low	Mid-low	Mid-low	Mid-low	Mid-low	Mid
3	0.2	0.3	0.5	Low	Low	Low	Low	Mid-low	High

change in l_s also increases considerably. Apart from that, at steeper γ and high h, the data band spreads over a range of 0.05 mm, suggesting that the variations of v_c can cause deviations in the contact length l_c by up to 0.05 mm under similar conditions of high h and steep γ.

The maximum temperature T_{cmax} increases with h in a nearly linear fashion across varied v_c conditions. In Fig. 20(c)(right) a relatively linear relationship is observed between h and T_{cmax}, particularly at elevated values of h, suggesting a consistent rate of change in T_{cmax} with h. Nevertheless, there is a notable non-linearity at the lower values of the h, particularly at low v_c conditions. Another noteworthy point to discuss is that, the new analytical model (see Fig. 20(c)(left)) initially developed for the underperforming region, successfully replicates the trend for the other conditions as well. This suggests that the new analytical model could be used to predict the full range of maximum contact temperature T_{cmax}. The downside is that this model does not account for the subtle effects of variations in γ, which is why the data band representing these variations is absent.

3.4.2. A holistic analysis of combined input parameter effects inspired by ternary plots

In Fig. 21, six ternary plots describes the simultaneous effects of all three input parameters on the outputs. However, to make use of this visualization method, the input parameters were normalized over the range of process parameters. The normalized values and their corresponding real values are also displayed in the same figure. The following section discusses the key interpretation of Fig. 21:

Cutting Force F_c and Passive Force F_p - It can be observed that, towards the left corner of the plot, F_c increases significantly with higher uncut chip thickness (h) and lower rake angles (γ).This observation aligns well with the findings presented in Fig. 19. Towards the top corner of the plot, higher v_c combined with lower h and steeper γ tends to reduce F_c. Apart from that, the ternary plot for F_c shows a relatively smooth gradient, and it steadily increases along the axis of uncut chip thickness (h). This trend further confirms the earlier observations in Figs. 18 and 19. A probable cause behind this characteristic is that this force is directly responsible for overcoming the material's resistance to being cut. As a result, F_c is directly influence by the amount of material removed, which is determined by the uncut chip thickness h, as mentioned in Section 3.3. A similar trend is also observed for the passive force F_p. It increases with larger h and higher negative rake angles also contributes to high F_p. That said, the F_p exhibits less continuous gradient than F_c. In certain force values there are abrupt changes, indicating that the passive force is more sensitive to other factors like material flow and frictional effects.

Contact Length l_c and Stick Length l_s - In Fig. 21(c) the combined effect of high uncut chip thickness h and high negative rake angle γ produces the highest contact length l_c values. Cutting velocity (located at the top of the ternary figure) has a complex influence on contact length that changes according to how the other two factors are combined. According to Altintas [72], the velocity at which the deformed chip slides at the rake face can be represented as

$$v_{chip} = \frac{h}{h_c} v_c = \frac{\sin(\phi_c)}{\cos(\phi_c - \gamma)} v_c \tag{7}$$

where ϕ_c is the shear angle designated to define the angle between the direction of the cutting velocity (v_c) and the shear plane. As can be seen in Eq. (7) the chip velocity v_{chip} is proportional to cutting velocity v_c. Hence, at higher cutting speeds, the chip should exhibit a greater chip velocity. However, the analysis shown in Fig. 21(c) demonstrates that if h is substantially high and γ is very negative, the impact of v_c is less noticeable.

As anticipated, the stick length l_s displayed a trend similar to that of the contact length l_c. Assuming a constant tool width, a higher uncut chip thickness h and a negative rake angle γ removes more material, thereby increases the chip area. These conditions also lead to a rise in the normal force exerted, which significantly increases the maximum normal stress. As discussed in Section 3.3, this increase in maximum normal stress allows the material to adhere to the tool over a longer span until the shear strength S_1 equals the frictional stress $\mu\sigma_n$. This analysis, therefore, confirms the earlier description of the stick length. Additionally, it can be observed in the top corner of Fig. 21(d), an increase in the value of v_c, a high negative value of γ, and a low value of h results in a reduction of stick length l_s due to the enhanced thermal softening of the material caused by high v_c.

Maximum Normal Stress $\sigma_{n\max}$ and Maximum Contact Temperature $T_{c\max}$ - Similar to the previous contact properties high h produces higher $\sigma_{n\max}$ values and high negative γ raises the resistance to chip flow, which increases the cutting force's normal component, leading to higher stress at the tool chip contact. It is obvious that extreme conditions of these two input parameters will maximize $\sigma_{n\max}$, increasing the risk of tool fracture. One important finding, nevertheless, is that in Fig. 21(e) a noticeable yellow strip is observed along the uncut chip thickness (h) axis at 0.2 normalized value (actual value - 0.056 mm). This suggests that an approximate value of 0.05 mm uncut chip thickness (h) is crucial to maintain the $\sigma_{n\max}$ below 2000 MPa, regardless of the values of v_c and γ. Unlike the earlier five properties, the maximum temperature is the sole contact property that exhibits a gradient inclination at a different angle. As discussed in Section 3.3, since v_c increases friction power P_u, and subsequently T_c, Fig. 21(f) also confirms

Normalised values	0	0.2	0.4	0.6	0.8	1
Uncut Chip Thickness (mm)	0.02	0.056	0.092	0.128	0.164	0.2
Rake Angle (°)	-35	-28	-21	-14	-7	0
Cutting Velocity (m/min)	100	120	140	160	180	200

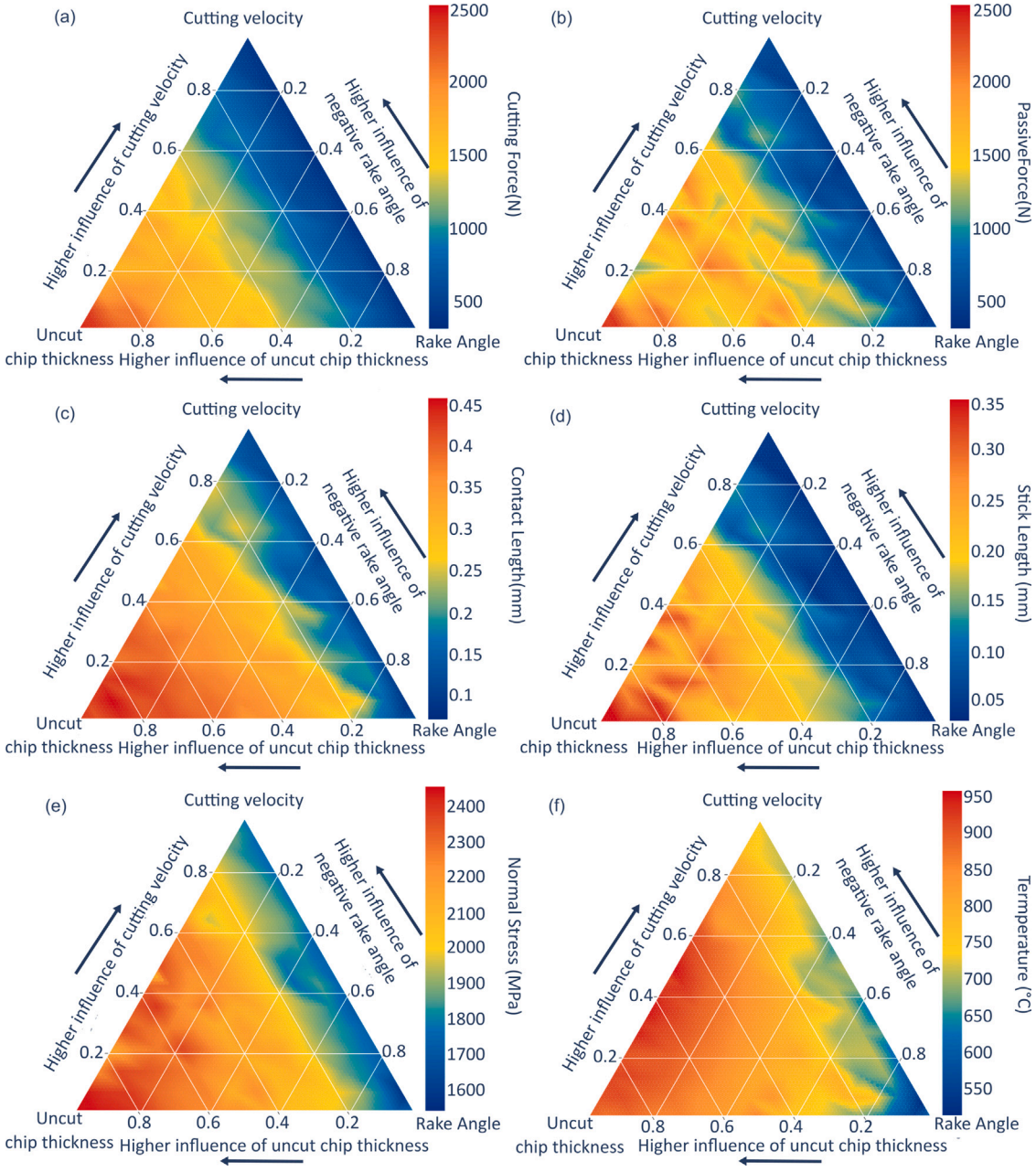

Fig. 21. Study of combined effect of all input parameters on thermo-mechanical properties (a) F_c cutting force, (b) F_p passive force, (c) l_c contact length, (d) l_s stick length, (e) $\sigma_{n\max}$ maximum normal contact pressure, (f) $T_{c\max}$ maximum contact temperature.

that maximum contact temperature T_c increases significantly with higher v_c. That said, uncut chip thickness h do also play a critical role in increasing T_c. While rake angle γ does not directly contribute to lowering the T_c, the low temperatures observed towards the bottom right corner of Fig. 21(f) suggest that using a steeper γ can be beneficial. If maintaining a lower T_c is necessary for improving the surface finish of the machined part and preserving tool integrity, it is advisable to choose a steeper γ. Based on the

ternary plots, an in-depth analysis is presented in Table 7, providing an overview of three different machining conditions and their holistic effects on the contact properties.

3.5. Prediction of cutting forces — Gear skiving

After the successful validation of the developed models for the interaction zone between the tool and AISI4140 and their associated usability for predicting thermo-mechanical loads, the first use of skiving is demonstrated. Fig. 22 vertical shows three discrete time steps of the gear skiving process under consideration according to Table 2. The determined local load parameters from the obtained models of the normal stress σ_n, temperature T_c and sliding velocity v_s are shown horizontally. The result of time step 30 shows the characteristic of the gear skiving process. The chip formation starts at the leading flank (LF) as well as at the point between the trailing flank (TF) and the tool tip. The following time step 60 is showing three separate chip formation zones during the tool engagement. The chip formation of the LF is widened compared to time step 30 to the tool tip. Further the tool tip as well as the TF is showing a zone of influence. The last presented time step 90 is showing the vis-a-vis behaviour compared to time step 30 where the outermost part of the TF and the part between the LF and tool tip is under the load of chip formation. The following observations can be described for the individual time steps:

- **Time step 30** — The zone of influence at the beginning of the gear skiving process is dominated by small uncut chip thickness, moderate negative rake angles, therefore the locally predicted contact length is in agreement with the observed results. In detail for the TF the maximum predicted normal stress $\sigma_{n_{max}} = 1586$ MPa, the contact temperature $T_{c_{max}} = 492$ °C and sliding velocity $v_{s_{max}} = 1956$ mm/s with the contact length $l_c = 0.09$ mm with the local determined process parameters at the x-value of x = 0.259 mm of $v_c = 118.1$ m/min, $h = 0.0172$ mm and $\gamma = -5.37$ °. For the maximum values of the LF with the local determined parameters of $v_c = 113.8$ m/min, $h = 0.0722$ mm and $\gamma = -4.19°$ at the tool location x = −1.28 mm the highest contact length is determined as $l_c = 0.2$ mm with the maximum temperature $T_{c_{max}} = 663$ °C, $\sigma_{n_{max}} = 1711$ MPa and $v_{s_{max}} = 1865$ mm/s.
- **Time step 60** — For the time step under investigation, the highest local loading can be found, in regard to the process kinematics, in the area of the tip region. The point of the highest contact length with a value of $l_c = 0.25$ mm at the tool x = 0.23 mm with the process parameters $v_c = 126.4$ m/min, $h = 0.0715$ mm and $\gamma = -14.6°$ with a resulting $\sigma_{n_{max}} = 1836$ MPa, $T_{c_{max}} = 746$ °C and $v_{s_{max}} = 1836$ mm/s can be found at the region between the tool tip and TF. In addition to the tool tip, both the flanks of the tool are engaged, and the contact properties can be determined. It also shows the high complexity of chip formation during gear skiving. For the LF the highest predicted contact length can be found at x = −1.158 mm with $l_c = 0.1$ mm and $\sigma_{n_{max}} = 1596$ MPa, $T_{c_{max}} = 508$ °C and $v_{s_{max}} = 1936$ mm/s with the identified local parameter of $v_c = 118.96$ m/min, $h = 0.0222$ mm and $\gamma = -4.0°$ For the TF the maximum $l_c = 0.13$ mm for the local process parameter $v_c = 120.97$ m/min, $h = 0.0330$ mm and $\gamma = -8.0°$ with the maximum local values determined by the prediction models of $\sigma_{n_{max}} = 1530$ MPa, $T_{c_{max}} = 568$ °C and $v_{s_{max}} = 1975$ mm/s The time step also is a great example of the gear skiving process, which shows in general a smaller uncut chip thickness on the LF compared to the TF, further it also shows that the tool tip has the highest loading due to high negative rake angles as well as high uncut chip thicknesses.
- **Time step 90** — For the last time step shown in the gear skiving process, the zones under load were reduced to two dedicated areas with the highest loadings in the area between the tip and LF. Where the highest predicted $l_c = 0.18$ mm for the tool-point $x = -0.163$ mm with the maximum local loading of $\sigma_{n_{max}} = 1714$ MPa, $T_{c_{max}} = 665$ °C and $v_{s_{max}} = 2162$ mm/s for the process parameter of $v_c = 132.5$ m/min, $h = 0.04$ mm and $\gamma = -18.9°$, while for TF the highest $l_c = 0.16$ mm at the tool point and x = 1.19 mm with parameters of $v_c = 121.3$ m/min, $h = 0.045$ mm and $\gamma = -8.87°$. Moreover, the maximum predicted parameter of $\sigma_{n_{max}} = 1628$ MPa, $T_{c_{max}} = 617$ °C and $v_{s_{max}} = 1987$ mm/s.

Applying the developed prediction models for the entire time steps of the gear skiving process under investigation, allows to predict the cutting forces during the real process. With the prediction of the contact length l_c and the normal pressure distribution σ_n in combination with the Eq. (6) the forces in axial direction of the tool can be predicted. Fig. 23(a) shows the results of the prediction (yellow) and the experimental data (green) of the tenth in-feed of the process. The experimental recorded forces are described as the mean value (dashed line) and the minimum and maximum value, which are represented by the shaded green area. In a side-by-side comparison of the prediction and the experiment, it could be determined that the force up to a timestamp of 1.8 ms is underestimated by the prediction with the linked calculation by about 10% compared to the experiment. Until the process time 2.14 ms the force then is predicted within the force measurements gathered by the experiments. In the middle of the process time there is a deviation of the prediction to the experiment of 5%, while the predicted peak of the process is not located at the peak of the experimental data and is advanced by 0.2 ms. That being said, the last part of the process is predicted well by the developed procedure, resulting in a R^2 value of 0.96.

Fig. 23 shows the maximum values determined for each in-feed of the process in comparison to the predicted values. The graph shows that up until the 4th in-feed the prediction underestimates the forces. The first two in-feeds show the highest deviation of approximately 25%. Considering the minimum and maximum values of the experimental forces, the prediction is in good agreement after the 5th tool pass.

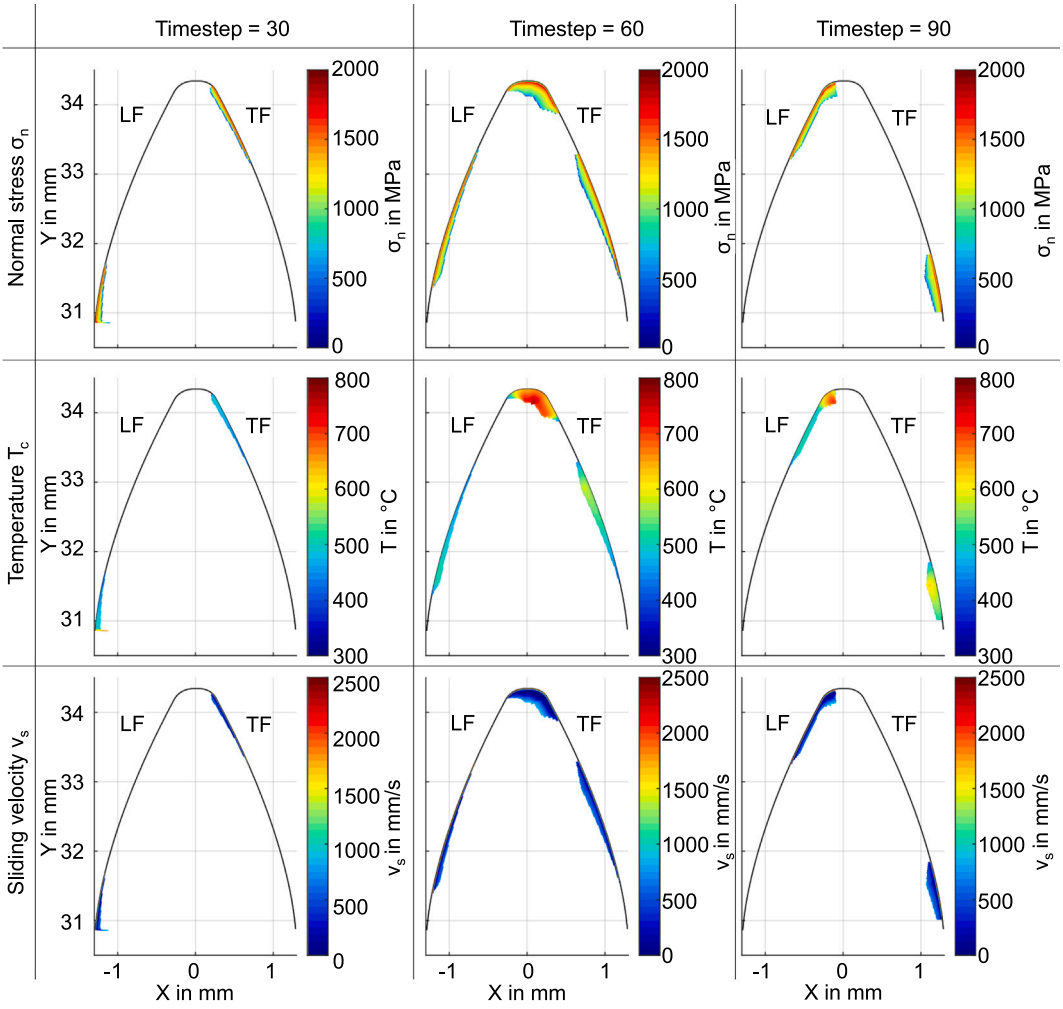

Fig. 22. Prediction of thermo-mechanical loading for Gear Skiving for discrete time steps.

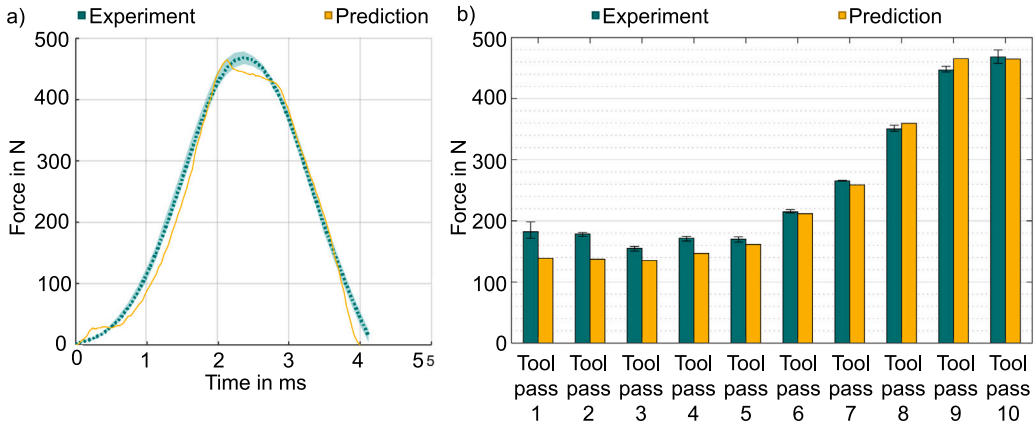

Fig. 23. (a) Force prediction using the developed prediction model in comparison to experimental forces (b) comparison of the highest cutting forces experiment and prediction.

4. Conclusion

This study has presented a comprehensive investigation of the possibilities to predict the thermo-mechanical properties in the tool chip interaction zone of AISI 4140, by employing both numerical methods such as FEM and a multivariate regression approach. Integration of these methods proved to be effective in predicting the contact properties and interpreting the complex relationship between process parameters and thermo-mechanical outcomes. Finally applying the developed models to the prediction of thermo-mechanical loading and forces of the gear skiving process. The key findings of the work are:

- **Computational Optimization** - The automated FEM tool demonstrates a workflow to simulate orthogonal cutting with simulation times of 45–120 min for depending on input parameters. Subsequently, the application of regression modelling significantly reduced computational demands. A database of 3375 test cases was generated in 112.5 min, resulting in a 2460-fold reduction in simulation time.
- **Validation of Numerical Model** — The numerical model has an average deviation of 5% for both cutting forces (F_c) and contact length (l_c), provides reliable predictions that closely match experimental results. It was observed that the passive force (F_p) has a higher average deviation of 12%, which is at par with the state-of-the-art regarding the selected material model. The simulation model slightly overestimates the contact temperature T_{cmax} across all test cases. The overestimation is attributed to the exclusion of heat transfer coefficients between the tool and thermocouple in the model. Despite this, the results are considered satisfactory. The simulated chip thickness h_c is slightly overestimated, but is well within the acceptable limits. The maximum deviation for h_c is 20%, or up to 30 μm, while the average deviation is 12%.
- **Evaluation of Regression Models** - By comparing the regression predictions with the simulated data from 200 simulations, six distinct regression models were assessed. The degree to which data points matched a reference line was used to determine accuracy, and the majority of models demonstrated good resilience. For additional assessment, a Monte Carlo design with 50 test cases was employed, with an emphasis on predicting variations in unit values as opposed to percentages. Nevertheless, it was noted that in extreme γ and h circumstances, three of the six contact characteristics (T_{cmax}, l_c, and l_s) were unable to extrapolate appropriate values. In areas where the original models failed, analytical models were created to increase the forecast accuracy of contact length (l_c), stick length (l_s), and maximum temperature (T_{cmax}).
- **Correlation Investigation** - The correlation study using the generated data revealed that among the considered process parameters uncut chip thickness (h) had the greatest impact on the contact properties, particularly on contact length l_c, where cutting velocity (v_c) and rake angle γ has little to no influence. However, cutting velocity (v_c) has a notable positive correlation with maximum contact temperature (T_{cmax}) and minimal relationship with rest of the contact properties. A moderate negative correlation is observed in between rake angle (γ) and outputs like maximum contact normal stress (σ_{nmax}) and passive force (F_p). A slight increase in stick length (l_s) is experienced as the negativity of rake angle (γ) increases.
- **Combined Effect Analysis** - The inbuilt multivariate prediction models offer a valuable holistic framework, confirming that this approach makes it possible to replace conventional computational models with data-driven approaches, by maintaining an updated database. The quick prediction capability of regression models opens up tremendous opportunities for real-time optimization of machining parameters. The interaction plots and ternary diagrams were used to visualize the simultaneous effects of all three input parameters (h, γ, v_c) on the output parameters (F_c, F_p, l_c, l_s, σ_{nmax}, T_{cmax}). The results indicated that the forces (F_c, F_p), the contact length (l_c) and the maximum contact temperature (T_{cmax}) increases linearly with h, but vary with γ. Nevertheless, a minimal non-linearity is observed for l_c at the lower values of h, particularly for conditions that correspond to higher negative rake angles (γ). Conversely, the contact temperature T_{cmax} demonstrates distinct non-linear characteristics at the lower end of the h, especially at low v_c conditions. Additionally, l_s and σ_{nmax} also exhibit a positive correlation with h. At lower values of h, both l_s and σ_{nmax} demonstrate rapid increase. As h increases, the rate of change of l_s and σ_{nmax} decreases, suggesting that an increase in h does not necessarily lead to a corresponding increase in these output properties. This suggests that their behaviour is influenced by other factors as well. Finally, three distinct combinations of h, γ and v_c were examined in order to analyse the collective impacts on the considered output contact properties.
- **Application in Gear Skiving Process** — The prediction of thermo-mechanical loadings of a representative gear skiving process using the developed models seems to be a promising way to predict the local acting loads. Therefore, with the knowing and fast prediction of the acting loadings, it can lead to a process optimization bot only based on kinematic calculation but also considering the physical determined loadings for a more effective and sustainable process design. Furthermore, in the past, only 3D-chip formation simulation were able to predict the thermo-mechanical loading. That said, and the comparison of chip formation of gear skiving processes, the developed method in combination with the well validated prediction models leads to a decrease of predicting the loadings by the factor of approximately 360 times.

5. Outlook

This study proposes an optimized automated workflow for generating finite element (FE) models and regression models under different cutting parameters, providing a robust foundation for investigating tool-chip interactions. It is acknowledged that the suggested methodology could be extended beyond the scope of the study. The proposed streamlined workflow can be tuned to generate different kinds of dataset for a more in-depth investigation of the contact zone. The future research possibilities utilizing the workflow:

- The utilization of an automated workflow to predict material-dependent JC-parameters for improved material modelling. As suggested by Stampfer et al. [30], the prediction of JC-Parameters by experiments can be implemented to get further insights of the influence of material properties on the estimation values.
- Extend existing databases, experiment- and simulation wise to extend the prediction of different processes e.g. high-speed-cutting.
- Expand the input database to simulate thermo-mechanical loading for a range of workpieces and tool materials.
- The impact of other process parameters could also be explored, like cutting-edge rounding, tool geometry, or coatings on the tool-chip interface.
- Analysing forces, temperature, and stress distributions on the machined layer to predict surface modification like micro-hardness variations and their relation to thermo-mechanical loading.
- Incorporating cutting fluids in simulations to evaluate their influence on forces, temperatures, and tool wear.
- Utilizing Usui's wear equation to predict tool wear during skiving, since the needed input parameter of Usui et al. [75] is provided by the proposed modelling.

$$\frac{dW}{dt} = A\sigma_n V_s e^{-\frac{B}{T}} \tag{8}$$

where σ_n, V_s, and T represent normal stress, sliding velocity, and temperature, respectively.

Acknowledgements

The authors gratefully acknowledge the funding of this work within the Priority Program 2231 "Efficient Cooling, Lubrication and Transport-Coupled Mechanical and Fluid Dynamic Simulation Methods for Efficient Production Processes (FLUSIMPRO)" by the German Research Foundation (DFG) – Project No. 439954775.

Data availability

Data will be made available on request.

References

[1] H. Narita, H. Fujimoto, Analysis of environmental impact due to machine tool operation, Int. J. Autom. Technol. 3 (1) (2009) 49–55, http://dx.doi.org/10.20965/ijat.2009.p0049.
[2] G. Shao, D. Kibira, K. Lyons, A virtual machining model for sustainability analysis, 2010, pp. 875–883, URL https://doi.org/10.1115/DETC2010-28743.
[3] J. Riezebos, W. Klingenberg, Advancing lean manufacturing, the role of IT, Comput. Ind. 60 (4) (2009) 235–236, http://dx.doi.org/10.1016/j.compind.2009.01.005, URL https://www.sciencedirect.com/science/article/pii/S0166361509000219.
[4] C. Cimino, E. Negri, L. Fumagalli, Review of digital twin applications in manufacturing, Comput. Ind. 113 (2019) 103130, http://dx.doi.org/10.1016/j.compind.2019.103130, URL https://www.sciencedirect.com/science/article/pii/S0166361519304385.
[5] P.J. Arrazola, F. Meslin, S. Marya, Numerical cutting sensitivity study of tool-chip contact, Mater. Sci. Forum 426–432 (2003) 4519–4524, http://dx.doi.org/10.4028/www.scientific.net/MSF.426-432.4519, URL https://www.scientific.net/MSF.426-432.4519.
[6] H. Miguélez, R. Zaera, A. Rusinek, A. Moufki, A. Molinari, Numerical modelling of orthogonal cutting: Influence of cutting conditions and separation criterion, J. de Phys. IV (Proceedings) 134 (2006) 417–422, http://dx.doi.org/10.1051/jp4:2006134064, URL http://www.edpsciences.org/10.1051/jp4:2006134064.
[7] J.C. Outeiro, D. Umbrello, R. M'Saoubi, Experimental and numerical modelling of the residual stresses induced in orthogonal cutting of AISI 316L steel, Int. J. Mach. Tools Manuf. 46 (14) (2006) 1786–1794, http://dx.doi.org/10.1016/j.ijmachtools.2005.11.013, URL https://www.sciencedirect.com/science/article/pii/S0890695505003081.
[8] N.A. Abukhshim, P.T. Mativenga, M.A. Sheikh, Heat generation and temperature prediction in metal cutting: A review and implications for high speed machining, Int. J. Mach. Tools Manuf. 46 (7) (2006) 782–800, http://dx.doi.org/10.1016/j.ijmachtools.2005.07.024, URL https://www.sciencedirect.com/science/article/pii/S089069550500180X.
[9] M. Barge, H. Hamdi, J. Rech, J.-M. Bergheau, Numerical modelling of orthogonal cutting: influence of numerical parameters, J. Mater. Process. Technol. 164–165 (2005) 1148–1153, http://dx.doi.org/10.1016/j.jmatprotec.2005.02.118, URL https://www.sciencedirect.com/science/article/pii/S0924013605002256.
[10] M.E. Merchant, Mechanics of the metal cutting process. I. Orthogonal cutting and a type 2 chip, J. Appl. Phys. 16 (5) (1945) 267–275, URL https://doi.org/10.1063/1.1707586.
[11] B. Borsos, A. Csörgő, A. Hidas, B. Kotnyek, A. Szabó, A. Kossa, G. Stépán, Two-dimensional finite element analysis of turning processes, Period. Polytech. Mech. Eng. 61 (1 SE -) (2017) 44–54, http://dx.doi.org/10.3311/PPme.9283, URL https://pp.bme.hu/me/article/view/9283.
[12] F. Ducobu, E. Rivière-Lorphèvre, E. Filippi, On the importance of the choice of the parameters of the johnson-cook constitutive model and their influence on the results of a Ti6Al4V orthogonal cutting model, Int. J. Mech. Sci. 122 (2017) 143–155, http://dx.doi.org/10.1016/j.ijmecsci.2017.01.004, URL https://www.sciencedirect.com/science/article/pii/S0020740316303381.
[13] H. Chandrasekaran, R. M'Saoubi, H. Chazal, Modelling of material flow stress in chip formation process from orthogonal milling and split hopkinson bar tests, Mach. Sci. Technol. 9 (1) (2005) 131–145, http://dx.doi.org/10.1081/MST-200051380.
[14] P.J. Arrazola, T. Özel, D. Umbrello, M. Davies, I.S. Jawahir, Recent advances in modelling of metal machining processes, CIRP Ann 62 (2) (2013) 695–718, http://dx.doi.org/10.1016/j.cirp.2013.05.006, URL https://www.sciencedirect.com/science/article/pii/S0007850613001960.
[15] N. Troß, J. Brimmers, T. Bergs, Approach for multiscale modeling the thermomechanical tool load in gear hobbing, Forsch. Im Ingen. 86 (3) (2022) 627–638, URL https://doi.org/10.1007/s10010-021-00531-5.
[16] X.P. Li, K. Iynkaran, A.Y.C. Nee, A hybrid machining simulator based on predictive machining theory and neural network modelling, J. Mater. Process. Technol. 89–90 (1999) 224–230, http://dx.doi.org/10.1016/S0924-0136(99)00068-0, URL https://www.sciencedirect.com/science/article/pii/S0924013699000680.

[17] M. Zadshakoyan, V. Pourmostaghimi, Genetic equation for the prediction of tool–chip contact length in orthogonal cutting, Eng. Appl. Artif. Intell. 26 (7) (2013) 1725–1730, http://dx.doi.org/10.1016/j.engappai.2012.10.016, URL https://www.sciencedirect.com/science/article/pii/S0952197612002850.

[18] D. Wu, C. Jennings, J. Terpenny, R.X. Gao, S. Kumara, A comparative study on machine learning algorithms for smart manufacturing: Tool wear prediction using random forests, J. Manuf. Sci. Eng. 139 (7) (2017) URL https://doi.org/10.1115/1.4036350.

[19] B. Vargas, M. Zapf, J. Klose, F. Zanger, V. Schulze, Numerical modelling of cutting forces in gear skiving, Procedia CIRP 82 (2019) 455–460.

[20] B. Vargas, V. Schulze, Three-dimensional modeling of gear skiving kinematics for comprehensive process design in practical applications, CIRP Ann 70 (1) (2021) 99–102, http://dx.doi.org/10.1016/j.cirp.2021.04.075.

[21] V. Schulze, C. Kühlewein, H. Autenrieth, 3D-FEM modeling of gear skiving to investigate kinematics and chip formation mechanisms, Adv. Mater. Res. 223 (2011) 46–55, http://dx.doi.org/10.4028/www.scientific.net/AMR.223.46.

[22] E. Guo, Z. Shi, L. Hu, E. Zhang, X. Ren, Design method of a multi-blade skiving tool for gear skiving, Mech. Mach. Theory 173 (2022) 104848, http://dx.doi.org/10.1016/j.mechmachtheory.2022.104848.

[23] A. Antoniadis, Gear skiving—CAD simulation approach, Computer- Aided Des. 44 (7) (2012) 611–616, http://dx.doi.org/10.1016/j.cad.2012.02.003.

[24] T. Bergs, A. Georgoussis, C. Löpenhaus, Development of a numerical simulation method for gear skiving, Procedia CIRP 88 (2020) 352–357, http://dx.doi.org/10.1016/j.procir.2020.05.061.

[25] X. Lin, Y. Liu, S. Sun, G. Jin, R. Hong, Prediction and optimization of gear skiving parameters and geometric deviations, Int. J. Adv. Manuf. Technol. 121 (5) (2022) 4169–4185, http://dx.doi.org/10.1007/s00170-022-09639-6.

[26] OpenSkiving, KIT Campus Transfer GmbH, 2024, URL https://openskiving.kit-campus-transfer.de/.

[27] F. Sauer, T. Arndt, V. Schulze, Tool wear development in gear skiving process of different quenched and tempered internal gears, 4th International Conference on Gear Production, VDI 2389 (2022) 1331–1343.

[28] T. Arndt, J. Klose, M. Gerstenmeyer, V. Schulze, Tool wear development in gear skiving process of quenched and tempered internal gears, Forsch. Im Ingenieurwesen 86 (3) (2022) 587–594, URL https://doi.org/10.1007/s10010-021-00544-0.

[29] A. Hilligardt, V. Schulze, A holistic approach for gear skiving design enabling tool load homogenization, CIRP Ann 71 (1) (2022) 85–88, http://dx.doi.org/10.1016/j.cirp.2022.03.029, URL https://www.sciencedirect.com/science/article/pii/S0007850622000312.

[30] B. Stampfer, G. González, E. Segebade, M. Gerstenmeyer, V. Schulze, Material parameter optimization for orthogonal cutting simulations of AISI4140 at various tempering conditions, Procedia CIRP 102 (2021) 198–203, http://dx.doi.org/10.1016/j.procir.2021.09.034, URL https://www.sciencedirect.com/science/article/pii/S2212827121007770.

[31] M. Agmell, A. Ahadi, J.-E. Ståhl, A fully coupled thermomechanical two-dimensional simulation model for orthogonal cutting: formulation and simulation, Proc. Inst. Mech. Eng. Part B: J. Eng. Manuf. 225 (10) (2011) 1735–1745, URL https://doi.org/10.1177/0954405411407137.

[32] T. Bergs, M. Hardt, D. Schraknepper, Determination of johnson-cook material model parameters for AISI 1045 from orthogonal cutting tests using the downhill-simplex algorithm, Procedia Manuf. 48 (2020) 541–552, http://dx.doi.org/10.1016/j.promfg.2020.05.081, URL https://www.sciencedirect.com/science/article/pii/S235197892031533X.

[33] L. Ellersiek, C. Menze, F. Sauer, B. Denkena, H.-C. Möhring, V. Schulze, Evaluation of methods for measuring tool-chip contact length in wet machining using different approaches (microtextured tool, in-situ visualization and restricted contact tool), Prod. Eng. 16 (5) (2022) 635–646, URL https://doi.org/10.1007/s11740-022-01127-w.

[34] MSCMarc, Hexagon AB, 2024, URL https://hexagon.com/products/marc.

[35] F. Klocke, H.-W. Raedt, S. Hoppe, 2D-FEM simulation of the orthogonal high speed cutting process, Mach. Sci. Technol. 5 (3) (2001) 323–340, URL https://doi.org/10.1081/MST-100108618.

[36] G. González, E. Segebade, F. Zanger, V. Schulze, FEM-based comparison of models to predict dynamic recrystallization during orthogonal cutting of AISI 4140, Procedia CIRP 82 (2019) 154–159.

[37] F. Sauer, A. Codrignani, M. Haber, K. Falk, L. Mayrhofer, C. Schwitzke, M. Moseler, H.-J. Bauer, V. Schulze, Multiscale simulation approach to predict the penetration depth of oil between chip and tool during orthogonal cutting of AISI 4140, Procedia CIRP 117 (2023) 426–431, http://dx.doi.org/10.1016/j.procir.2023.03.072, URL https://www.sciencedirect.com/science/article/pii/S2212827123002044. 19th CIRP Conference on Modeling of Machining Operations.

[38] V. Schulze, F. Bleicher, C. Courbon, M. Gerstenmeyer, L. Meier, J. Philipp, J. Rech, J. Schneider, E. Segebade, A. Steininger, K. Wegener, Determination of constitutive friction laws appropriate for simulation of cutting processes, CIRP J. Manuf. Sci. Technol. 38 (2022) 139–158, http://dx.doi.org/10.1016/j.cirpj.2022.04.008, URL https://www.sciencedirect.com/science/article/pii/S1755581722000712.

[39] G. González, E. Segebade, F. Zanger, V. Schulze, FEM-based comparison of models to predict dynamic recrystallization during orthogonal cutting of AISI 4140, Procedia CIRP 82 (2019) 154–159, http://dx.doi.org/10.1016/j.procir.2019.04.061, URL https://www.sciencedirect.com/science/article/pii/S2212827119306754. 17th CIRP Conference on Modelling of Machining Operations (17th CIRP CMMO).

[40] E. Segebade, D. Kümmel, F. Zanger, J. Schneider, V. Schulze, Influence of cutting edge asymmetry on grain refinement of Ti6Al4V, Procedia CIRP 71 (2018) 232–237, http://dx.doi.org/10.1016/j.procir.2018.05.065, URL https://www.sciencedirect.com/science/article/pii/S2212827118306930. 4th CIRP Conference on Surface Integrity (CSI 2018).

[41] E. Segebade, M. Gerstenmeyer, F. Zanger, V. Schulze, Cutting simulations using a commercially available 2D/3D FEM software for forming, Procedia CIRP 58 (2017) 73–78, http://dx.doi.org/10.1016/j.procir.2017.03.195, URL https://www.sciencedirect.com/science/article/pii/S2212827117303773. 16th CIRP Conference on Modelling of Machining Operations (16th CIRP CMMO).

[42] C. Grimm, C. Menze, J. Saelzer, F. Sauer, R. Eisseler, H.-C. Möhring, V. Schulze, A. Zabel, E. Uhlmann, Reproducibility analysis for different numerical models and experimental setups in dry orthogonal cutting of AISI 4140 steel, Procedia CIRP 128 (2024) 650–655, http://dx.doi.org/10.1016/j.procir.2024.04.018, URL https://www.sciencedirect.com/science/article/pii/S2212827124007455. 34th CIRP Design Conference.

[43] J. Schwalm, F. Mann, G. González, F. Zanger, V. Schulze, Finite element simulation of the process combination hammering turning, Procedia CIRP 117 (2023) 110–115, http://dx.doi.org/10.1016/j.procir.2023.03.020, URL https://www.sciencedirect.com/science/article/pii/S221282712300152X. 19th CIRP Conference on Modeling of Machining Operations.

[44] F. Richter, Die physikalischen eigenschaften der stähle – das 100-stähle-programm, teil I: Tafeln und bilder, 2015.

[45] G.S. Sarmiento, J.F. Bugna, L.C.F. Canale, R.M.M. Riofano, R.A. Mesquita, G.E. Totten, A.C. Canale, Modeling quenching performance by the kuyucak method, Mater. Sci. Eng.: A 459 (1) (2007) 383–389, http://dx.doi.org/10.1016/j.msea.2007.01.025.

[46] G.R. Johnson, W.H. Cook, Fracture characteristics of three metals subjected to various strains, strain rates, temperatures and pressures, Eng. Fract. Mech. 21 (1) (1985) 31–48, http://dx.doi.org/10.1016/0013-7944(85)90052-9, URL https://www.sciencedirect.com/science/article/pii/0013794485900529.

[47] F.J. Zerilli, R.W. Armstrong, Dislocation-mechanics-based constitutive relations for material dynamics calculations, J. Appl. Phys. 61 (5) (1987) 1816–1825, URL https://doi.org/10.1063/1.338024.

[48] A. Svoboda, D. Wedberg, L.-E. Lindgren, Simulation of metal cutting using a physically based plasticity model, Modelling Simul. Mater. Sci. Eng. 18 (7) (2010) 075005, URL http://dx.doi.org/10.1088/0965-0393/18/7/075005.

[49] T. Özel, The influence of friction models on finite element simulations of machining, Int. J. Mach. Tools Manuf. 46 (5) (2006) 518–530, http://dx.doi.org/10.1016/j.ijmachtools.2005.07.001, URL https://www.sciencedirect.com/science/article/pii/S0890695505001550.

[50] G. Shi, X. Deng, C. Shet, A finite element study of the effect of friction in orthogonal metal cutting, Finite Elem. Anal. Des. 38 (9) (2002) 863–883, http://dx.doi.org/10.1016/S0168-874X(01)00110-X, URL https://www.sciencedirect.com/science/article/pii/S0168874X0100110X.

[51] R.R. Reeber, K. Wang, Thermophysical properties of α-tungsten carbide, J. Am. Ceram. Soc. 82 (1) (1999) 129–135, URL https://doi.org/10.1111/j.1151-2916.1999.tb01732.x.
[52] G.S. Upadhyaya, Materials science of cemented carbides — an overview, Mater. Des. 22 (6) (2001) 483–489, http://dx.doi.org/10.1016/S0261-3069(01)00007-3, URL https://www.sciencedirect.com/science/article/pii/S0261306901000073.
[53] W.A. Kayser, Einflussfaktoren auf den Eigenspannungszustand in Hartmetall (Ph.D. thesis), Vol. 19, RWTH Aachen University, Düren, 2019, http://dx.doi.org/10.18154/RWTH-2019-10477, 1 Online–Ressource (XVII, 188 Seiten) : Illustrationen, Diagramme. URL https://publications.rwth-aachen.de/record/771904.
[54] H. Holey, F. Sauer, P.B. Ganta, L. Mayrhofer, M. Dienwiebel, V. Schulze, M. Moseler, Multiscale parametrization of a friction model for metal cutting using contact mechanics, atomistic simulations, and experiments, Tribol. Lett. 72 (4) (2024) 113, URL https://doi.org/10.1007/s11249-024-01906-9.
[55] J. Lorentzon, N. Järvstråt, Modelling tool wear in cemented-carbide machining alloy 718, Int. J. Mach. Tools Manuf. 48 (10) (2008) 1072–1080, http://dx.doi.org/10.1016/j.ijmachtools.2008.03.001, URL https://www.sciencedirect.com/science/article/pii/S089069550800045X.
[56] J. Han, M. Kamber, J. Pei, Data Mining Concepts and Techniques, Morgan Kaufmann Publishers, 2017.
[57] R. Lostado, F. Martínez-De-Pisón, A. Pernía, F. Alba, J. Blanco, Combining regression trees and the finite element method to define stress models of highly non-linear mechanical systems, J. Strain Anal. Eng. Des. 44 (6) (2009) 491–502.
[58] P. Dong, H. Peng, X. Cheng, Y. Xing, X. Zhou, D. Huang, A random forest regression model for predicting residual stresses and cutting forces introduced by turning IN718 alloy, in: Conference on Computation, Communication and Engineering (ICCCE 2019), 2019, http://dx.doi.org/10.1109/ICCCE48422.2019, URL https://ieeexplore.ieee.org/servlet/opac?punumber=8981714.
[59] B. Peng, T. Bergs, D. Schraknepper, F. Klocke, B. Döbbeler, A hybrid approach using machine learning to predict the cutting forces under consideration of the tool wear, Procedia Cirp 82 (2019) 302–307.
[60] B. Vargas, M. Zapf, J. Klose, F. Zanger, V. Schulze, Numerical modelling of cutting forces in gear skiving, Procedia CIRP 82 (2019) 455–460, http://dx.doi.org/10.1016/j.procir.2019.04.039, URL https://www.sciencedirect.com/science/article/pii/S2212827119306535.
[61] S. Arlot, A. Celisse, A survey of cross-validation procedures for model selection, Stat. Surv. 4 (none) (2010) http://dx.doi.org/10.1214/09-SS054.
[62] F.A.C. Viana, A tutorial on latin hypercube design of experiments, Qual. Reliab. Eng. Int. 32 (5) (2016) 1975–1985, http://dx.doi.org/10.1002/qre.1924, URL https://onlinelibrary.wiley.com/doi/abs/10.1002/qre.1924.
[63] S.C. Larson, The shrinkage of the coefficient of multiple correlation, J. Educ. Psychol. 22 (1) (1931) 45–55, http://dx.doi.org/10.1037/h0072400.
[64] B. Bergmann, B. Denkena, S. Beblein, T. Picker, FE-simulation based design of wear-optimized cutting edge roundings, J. Manuf. Mater. Process. 5 (4) (2021) 126, http://dx.doi.org/10.3390/jmmp5040126.
[65] N.N. Zorev, Inter-relationship between shear processes occurring along tool face and shear plane in metal cutting., Int. Res. Prod. Eng. N. Y.: (1963).
[66] C. Rubenstein, A simple theory of orthogonal cutting, Int. J. Mach. Tool Des. Res. 4 (3) (1965) 123–156, http://dx.doi.org/10.1016/0020-7357(65)90015-6, URL https://www.sciencedirect.com/science/article/pii/0020735765900156.
[67] L. Breiman, Random forests, Mach. Learn. 45 (1) (2001) 5–32, http://dx.doi.org/10.1023/A:1010933404324, URL https://link.springer.com/article/10.1023/a:1010933404324.
[68] I. Ghosal, G. Hooker, Boosting random forests to reduce bias; one-step boosted forest and its variance estimate, J. Comput. Graph. Statist. 30 (2) (2021) 493–502, http://dx.doi.org/10.1080/10618600.2020.1820345.
[69] O. Kienzle, Die bestimmung von kräften und leistungen an spanenden Werkzeugen und Werkzeugmaschinen, VDI-Z 94 (11) (1952) 299–305.
[70] V. Sivaraman, S. Sankaran, L. Vijayaraghavan, The effect of cutting parameters on cutting force during turning multiphase microalloyed steel, Procedia CIRP 4 (2012) 157–160, http://dx.doi.org/10.1016/j.procir.2012.10.028, URL https://www.sciencedirect.com/science/article/pii/S2212827112003198. 3rd CIRP Conference on Process Machine Interactions.
[71] M.R. Mustafa Özdemir, V. Yilmaz, Analysis and optimisation of the cutting parameters based on machinability factors in turning AISI 4140 steel, Can. Metall. Q. 61 (4) (2022) 407–417, arXiv:https://doi.org/10.1080/00084433.2022.2058154. URL https://doi.org/10.1080/00084433.2022.2058154.
[72] Y. Altintas, Manufacturing Automation: Metal Cutting Mechanics, Machine Tool Vibrations, and CNC Design, second ed., Cambridge University Press, Cambridge and New York, 2012.
[73] B. Karpuschewski, J. Kundrák, G. Varga, I. Deszpoth, D. Borysenko, Determination of specific cutting force components and exponents when applying high feed rates, Procedia CIRP 77 (2018) 30–33.
[74] M. Salehi, T. Schmitz, R. Copenhaver, R. Haas, J. Ovtcharova, Probabilistic sequential prediction of cutting force using kienzle model in orthogonal turning process, J. Manuf. Sci. Eng. 141 (1) (2019) 011009.
[75] E. Usui, T. Shirakashi, T. Kitagawa, Analytical prediction of cutting tool wear, Wear 100 (1) (1984) 129–151, http://dx.doi.org/10.1016/0043-1648(84)90010-3, URL https://www.sciencedirect.com/science/article/pii/0043164884900103.